D-150 Invited Paper

Combustion Science and Technology

ISSN: 0010-2202 (Print) 1563-521X (Online) Journal homepage: http://www.tandfonline.com/loi/gcst20

# Driving Mechanisms for Combustion Instability

William A. Sirignano

**To cite this article:** William A. Sirignano (2015) Driving Mechanisms for Combustion Instability, Combustion Science and Technology, 187:1-2, 162-205, DOI: 10.1080/00102202.2014.973801

**To link to this article:** http://dx.doi.org/10.1080/00102202.2014.973801

*Combust. Sci. Technol.*, 187: 162–205, 2015

ISSN: 0010-2202 print / 1563-521X online
DOI: 10.1080/00102202.2014.973801

Taylor & Francis
Taylor & Francis Group

# DRIVING MECHANISMS FOR COMBUSTION INSTABILITY

**William A. Sirignano**
*Department of Mechanical and Aerospace Engineering, University of California, Irvine, California, USA*

***The processes affecting the nonlinear acoustic stability of a combustor are examined in an overview fashion. Emphasis is placed on liquid-propellant rocket motors but other systems are briefly mentioned and some broadly applied principles and observations are discussed. A nonlinear wave equation is developed for a two-phase mixture and the roles of various terms in the equations are discussed. A review is made of various combustion processes, their associated characteristic times, and the impacts on stability in certain cases. Many relevant scales for length and time are identified. Special issues for supercritical and transcritical combustion are discussed. Bistable operational domains are shown to be present in some systems, making nonlinear triggering of an instability a possibility. Relations between the natural frequency of oscillation for the combustion chamber and the characteristic combustion times are identified with regard to impact on the combustor stability. The amplitude of the limit cycle and the transient time for limit-cycle development are related to the mean-flow Mach number. The role of shock-wave dissipation in amplitude determination is described.***

***Keywords***: Combustion instability; Continuous combustion; Unsteady combustion

## 1. INTRODUCTION

Combustion instability in rocket engines and other continuous-combustion engines has provided a major design challenge for the engineer and a substantial intellectual challenge to the researcher. It demands an understanding of unsteady combustion processes and nonlinear acoustical resonance. The researcher must address the intertwined, multidisciplinary issues of combustion, transport, fluid dynamics, acoustics, and nonlinear dynamics. While many examples in this discussion will be related to liquid-propellant rocket engines, not all are. More importantly, two points must be understood: (i) all acoustic oscillations in partially confined gaseous chambers relate to each other regardless of shape or application; and (ii) combustion processes, such as phase change, mixing, and oxidation, regardless of the particular combustion chamber in which they occur are related. Therefore, many principles and observations will have value for a range of combustor applications.

Received 15 August 2014; revised 20 September 2014; accepted 30 September 2014.
Published as part of the Special Issue in Honor of Professor Forman A. Williams on the Occasion of His 80th Birthday with Guest Editors Chung K. Law and Vigor Yang.
Address correspondence to William A. Sirignano, Dept. of Mechanical & Aerospace Engineering, University of California, Irvine, CA 92697-3975, USA. E-mail: sirignan@uci.edu
Color versions of one or more of the figures in the article can be found online at www.tandfonline.com/gcst.

There are two general types of acoustical combustion instability: "driven" instability and "self-excited" instability as noted by Culick (2006). He describes evidence in some solid-propellant rockets of the former (driven) type where vortex shedding (a more organized noise) causes kinematic waves (i.e., waves carried with the moving gas) of vorticity or entropy to travel to some point where an acoustical reflection occurs. The reflected wave causes more vortex shedding after traveling back and a cyclic character results. These driven types do not rely on acoustical chamber resonance and acoustical waves traveling upstream are the only type of consequence with kinematic waves only traveling downstream by the kinematic definition. They are much smaller in amplitude since the energy level is limited by the driving energy. This type of instability has also been observed in ramjet combustors but never in liquid rockets. They will not be addressed here. Self-excited instabilities are the primary type relevant to liquid-propellant rockets but also appear elsewhere. These instabilities involve an acoustical resonance, which relies on a coupling between the acoustical waves and the combustion process where energy is added in a cyclic fashion to the acoustically resonant gas in the combustion chamber.

It has been well established based on experiment and development-test experience (Harrje and Reardon, 1972) that three types of stability zones can be found: unconditionally stable operation where the amplitude of any disturbance (large or small) decays in time to the steady-state operation; unconditionally unstable operation where the amplitude of any disturbance (large or small) grows in time to a limit-cycle oscillation; and bistable operation where growth to a limit-cycle occurs for disturbance amplitudes above a specific threshold but decay to the steady state results for disturbances of a magnitude below the threshold.

The particular resonant mode is a characteristic of the particular combustion chamber and convergent portion of the nozzle. Any partially confined gas volume has an infinity of different theoretically possible resonant acoustic modes. These resonant mode oscillations and their frequencies are predictable by linear theory. They depend on chamber shape, boundary conditions for the chamber flow, and the field values for speed-of-sound and velocity vector through the chamber gas. The lowest frequency mode is identified as the fundamental mode while the other modes are overtones. Only in special situations are the overtones also harmonics of the fundamental mode; that is, their frequencies are integer multiples of the fundamental frequency. Generally, the harmonics are not predicted by linear theory to occur in isolated fashion. It is well known from the theory of nonlinear oscillations that, for many mechanical systems, nonlinear resonance can involve any of several developments: the generation of harmonics superimposed on the basic resonant mode; the simultaneous excitement of other resonant modes by transfer of energy among modes; and the transfer of energy to a subharmonic mode whose frequency is lower than the basic mode and related arithmetically to two or more resonant modes (e.g., the difference between two resonant frequencies).

These self-excited instabilities are not limited in amplitude by the energy of the initiation action; they find the energy within their own "macro" (i.e., chamber or acoustic wavelength scale) behavior as the oscillations grows and develops. So, the initiation can be micro-level (at least one order of magnitude smaller than chamber scale) but the instability becomes macro-level. These instabilities include those linear unstable (i.e., unconditionally unstable) situations where normal low-level engine noise is sufficient to initiate the instability oscillation and those triggered (i.e., conditionally stable or equivalently conditionally unstable) instabilities, which require a larger initial disturbance to initiate the nonlinear

oscillation. Physically, the rogue disturbance is some deviant behavior in the operation that has uncertainty with regard to location in the physical coordinates, duration, and magnitude. The deviant behavior "jolts" the steady-state behavior. Sometimes, there is a recovery and a return to the steady-state but, at other times, the development of the oscillation occurs with a growing of the oscillation amplitude until the limit cycle is reached. The needed jolt to initiate instability can sometimes come during a rapid start of the engine so that steady state never appears.

With the self-excited instability, a gradual and continuous change in some direction of operating conditions (e.g., mixture ratio or mass flow) or design (e.g., nozzle throat area or injector detail) could cause a variation through the several instability domains: unconditionally stable, conditionally stable, unconditionally unstable, and perhaps back to conditionally stable and unconditionally stable. Moderate (normal "steady-state" rumbling) noise might initiate the linear instability in certain operational domains and large disruptive noise (e.g., an experimental bomb, a large operational change, a large but temporary rogue injector blockage or injector exit vortex) might trigger the nonlinear instability in some other operational domain. In those cases, noise or disruptions are typically only initiators with modest energy levels compared to the energy of the ultimate oscillation. The initiators can be turned off or disappear naturally once the instability starts and the oscillation will remain and grow. That is, it is driven by a coupling between combustion and acoustics. The stochastic nature pertains only to the initiation mechanism, which moves the dynamics from the steady-state (or nonoscillatory starting transient) to a stable limit cycle (the periodic or chaotic nonlinear oscillation). The limit cycles and the equilibrium points are neither stochastic in nature nor stochastic with regard to the ultimate driving mechanism.

In order to drive a combustion instability, certain relations between the resonant frequency and the characteristic times associated with the combustion process are required. The limit-cycle amplitude of the oscillation will also be related to certain parameters describing the combustion process. In situations where triggering of an oscillation occurs, the threshold amplitude (or unstable-limit-cycle amplitude) will be related to certain combustion parameters. Certain damping mechanisms will also affect the behavior. An overview of these issues will be presented here. Examples will be chosen that are most familiar to the author. It is not claimed that a thorough review of the literature is being offered; rather, the focus will be on the underlying concepts. Obviously, the work of the author will find preference among the examples. For more detailed reviews of combustion instability, see Crocco and Cheng (1956), Harrje and Reardon (1972), Yang and Anderson (1995), and Culick (2006).

In the next section, we formulate the governing differential equations and boundary conditions in a general form for a two-phase flow undergoing chemical reaction and exchanges of mass, momentum, and energy between the phases. The third section develops those equations into a useful form for studying wave oscillations in a combustion chamber/convergent-nozzle configuration. The characteristic times associated with the injection and combustion processes and their connection with unstable oscillations are discussed in the fourth section. This subject relates to sub-grid models in large-eddy simulations (LES) for combustion chambers. In the fifth section, the factors determining the threshold for triggering and the limit-cycle amplitude are discussed. Then, a summary of key conclusions is given in the last section.

## 2. TWO-CONTINUA, TWO-PHASE FORMULATION

In this section, we will present the two-continua system of equations in the forms that are commonly used. It is noteworthy (Sirignano, 2005b, 2005a, 2010) that this general approach was first developed for specific application to longitudinal-mode liquid-propellant rocket engine combustion instability in the PhD dissertation of S.-I. Cheng working with L. Crocco (Crocco and Cheng, 1953, 1956). The basic concept developed there in the 1950s of two superimposed continuous fields has since been extended to dusty gases, bubbly flows, and flows through porous material. Properties are averaged over a sufficiently large neighborhood of any point that both carrier-fluid (continuous-phase) and discrete-phase properties exist at any point. Here, we use a three-dimensional (3D) version of the theory. This formulation is designed to address a common situation in a combustor where the gas is laden with droplets or particles, e.g., a spray combustion situation. In particular, averaging of properties is done over a neighborhood scale larger than droplet size or distance to nearest droplets. Exchanges of mass, momentum, and energy occur between the phases and must be tracked. The higher order quantities, which relate to differences between products (and a ratio) of averages and averages of products (and a ratio), are neglected in the following formulation. The bar symbol is used over the density in order to distinguish between bulk density and the mass per unit volume of the mixture. Details are provided by Sirignano (2010).

In the following discussion, we examine the various conservation principles for the gas and liquid phases. The hyperbolic nature of the liquid-phase equations and the consequences are examined. The interactions between the two phases will introduce many new length scales and time scales that can be consequential. These scales will be surveyed in section 4.

### 2.1. Mass Conservation

We consider the various forms of mass continuity or conservation equations for the gas and liquid phases. Mass conservation of individual chemical species or of individual classes of liquid droplets will also be considered. The conservation of droplet numbers will be explored. The gas-phase mass-conservation equation is:

$$\frac{\partial \bar{\rho}}{\partial t} + \frac{\partial}{\partial x_j}\left(\bar{\rho} u_j\right) = \dot{M} \tag{1}$$

The term on the right side does not appear if no mass is exchanged between the phases.

The liquid-phase mass-conservation equation is:

$$\frac{\partial \bar{\rho}_l}{\partial t} + \frac{\partial}{\partial x_j}\left(\bar{\rho}_l u_{l,j}\right) = -\dot{M} \tag{2}$$

where $\dot{M}$ is the mass vaporization rate per unit volume. Models for evaluating the vaporization rate $\dot{M}$ are required. As a result of vaporization, mass is not conserved for each phase but the mass of the mixture is conserved.

For a constant bulk liquid density $\rho_l$, $\bar{\rho}_l = (1-\theta)\,\rho_l$, where $\theta$ is the local volume fraction occupied by gas.

Consider now the gas-phase species-mass conservation. The integer index $m$ represents the particular species. The mass fraction $Y_m$ is described by:

$$\frac{\partial}{\partial t}\left(\bar{\rho}Y_m\right)+\frac{\partial}{\partial x_j}\left(\bar{\rho}u_jY_m\right)-\frac{\partial}{\partial x_j}\left(\bar{\rho}D\frac{\partial Y_m}{\partial x_j}\right)=\dot{M}_m+\bar{\rho}\dot{w}_m \tag{3}$$

where

$$\dot{M}=\sum_m\dot{M}_m=\sum_m\varepsilon_m\dot{M}\quad\sum_m\dot{w}_m=0$$

The mass diffusivity is assumed above to be the same for all species. Other options can be considered (Sirignano, 2010). $\varepsilon_m$ is the fractional vaporization rate for species $m$ and, for a quasi-steady gas phase, becomes a species mass-flux fraction. Obviously, $\sum_m\varepsilon_m=1$. Summation over all components in Eq. (3) yields the continuity equation (1). Therefore, if we have $N$ different species, only $N-1$ species-conservation equations need be solved together with Eq. (1).

## 2.2. Momentum Conservation

Now, let us consider the gas-phase momentum equation constructed in a simple form with neglect of body forces:

$$\frac{\partial}{\partial t}\left(\bar{\rho}u_i\right)+\frac{\partial}{\partial x_j}\left(\bar{\rho}u_ju_i\right)+\theta\frac{\partial\rho}{\partial x_i}-\theta\frac{\partial\tau_{ij}}{\partial x_j}=\dot{M}u_{l,i}-F_{Di} \tag{4}$$

where

$$\tau_{ij}=\mu\left(\frac{\partial u_i}{\partial x_j}+\frac{\partial u_j}{\partial x_i}-\frac{2}{3}\delta_{ij}\frac{\partial u_i}{\partial x_j}\right)$$

Equation (4) includes momentum sources and sinks due to droplet-vapor mass sources, reaction to droplet drag, and body forces on the gas. The drag and lift forces $F_{Di}$ in Eq. (4) can be related to the relative droplet–gas velocity and the droplet radius through the use of drag and lift coefficients. The equations are written for a laminar flow but turbulence modeling can be included in various ways. The simplest way would be to use an eddy viscosity $\mu_t$ in place of $\mu$ above.

The gas-phase momentum equation may be rewritten in a form where all effects of viscosity and mass and momentum exchanges appear as terms on the right side of the equation included together as a term $\dot{I}_i$ giving impulse per unit volume:

$$\frac{\partial}{\partial t}\left(\bar{\rho}u_i\right)+\frac{\partial}{\partial x_j}\left(\bar{\rho}u_ju_i\right)+\frac{\partial p}{\partial x_i}=\dot{I}_i \tag{5}$$

$$\dot{I}_i\equiv(1-\theta)\frac{\partial p}{\partial x_i}+\theta\frac{\partial\tau_{ij}}{\partial x_j}+\dot{M}u_{l,i}-F_{Di} \tag{6}$$

The liquid-phase momentum equation can be written as:

$$\frac{\partial}{\partial t}\left(\bar{\rho}_l u_{l,i}\right) + \frac{\partial}{\partial x_j}\left(\bar{\rho}_l u_{l,j} u_{l,i}\right) = -\dot{M} u_{l,i} + F_{Di} + \rho\,(1-\theta)\left[\frac{\partial u_i}{\partial t} + u_j \frac{\partial u_i}{\partial x_j}\right] \tag{7}$$

The last term in Eq. (7) implies that the acceleration that would have been given to the gas (if it were to exist in the fractional volume occupied by liquid), because of the pressure and the viscous stresses transferred from the neighboring gas, is transmitted as a force on the droplets. The neglected additions due to droplet interactions to the last term in Eq. (7) can be shown to be of the order of $(1-\theta)^2$. Note that the reaction to this force is already implied in the gas momentum equation (5) and need not be explicitly represented.

### 2.3. Energy Conservation

The perfect gas law is given as:

$$\theta p = \bar{\rho} R T \quad \bar{\rho} e = \bar{\rho} h - \theta p \tag{8}$$

The analysis could utilize a cubic form of the gas law that would apply better at high pressures. However, it will not change our major conclusions.

Then, the energy equation can be written as:

$$\begin{aligned} &\frac{\partial}{\partial t}\left(\bar{\rho} h\right) + \frac{\partial}{\partial x_j}\left(\bar{\rho} u_j h\right) - \frac{\partial}{\partial x_j}\left(\lambda \frac{\partial T}{\partial x_j}\right) - \frac{\partial}{\partial x_j}\left(\bar{\rho} D \sum_m h_m \frac{\partial Y_m}{\partial x_j}\right) \\ &= \theta \frac{\mathrm{d}p}{\mathrm{d}t} + \Phi + \bar{\rho} \sum_m \dot{w}_m Q_m - \dot{M} L_{eff} + \dot{M} h_s \end{aligned} \tag{9}$$

$L_{eff}$ is defined as the ratio of the conductive heat flux from gas to liquid surface to the vaporization mass flux. For the case where no heat passes to liquid interior (constant-liquid-temperature case), $L_{eff} = L$, the latent heat of vaporization. Note that,

$$h = \int_{T_{\mathrm{ref}}}^{T} c_p \mathrm{d}T' = \int_{T_{\mathrm{ref}}}^{T} \left[\sum_m Y_m c_{pm}\left(T'\right)\right] \mathrm{d}T'$$

and

$$\frac{dp}{dt} \equiv \frac{\partial p}{\partial t} + u_j \frac{\partial p}{\partial x_j} \tag{10}$$

For low Mach number, the viscous dissipation $\Phi$ can be neglected.

We reorganize the energy equation (9) to place the viscous term, terms related to conductive and mass transport of energy, and terms related to energy exchange between the phases into one source-sink term identified as $\dot{\varepsilon}$. Also, we define the energy conversion rate term to be:

$$E \equiv \bar{\rho} \sum_m \dot{w}_m Q_m \tag{11}$$

$$\frac{\partial}{\partial t}(\bar{\rho}h) + \frac{\partial}{\partial x_j}\left(\bar{\rho}u_j h\right) - \frac{\partial p}{\partial t} - u_j\frac{\partial p}{\partial x_j} - E = \dot{\varepsilon}$$
$$\dot{\varepsilon} \equiv (\theta - 1)\frac{dp}{dt} + \Phi + \frac{\partial}{\partial x_j}\left(\lambda\frac{\partial T}{\partial x_j}\right) + \frac{\partial}{\partial x_j}\left(\bar{\rho}D\sum_m h_m\frac{\partial Y_m}{\partial x_j}\right) - \dot{M}\,L_{eff} + \dot{M}\,h_s \tag{12}$$

The liquid-phase temperature will generally vary spatially and temporally within the liquid droplet. A Navier–Stokes solver or some approximate algorithms can be used to determine the temperature field in the droplet, including the surface temperature. In the special case of a uniform but time-varying liquid temperature in the droplet, an equation for the thermal energy contained in the droplet can be useful. If $e_l$ is the liquid internal energy per unit mass, then $\bar{\rho}e_l$ is the liquid internal energy per unit volume of mixture. In the case in which a spacial variation of temperature occurs in the droplet, $e_l$ could be considered as the average over the droplet. However, an equation for $e_l$ would not be so useful here since the difference between the average value and the surface value is not specified but yet the results are most sensitive to the surface temperature. Viscous dissipation can be neglected in the liquid-phase energy equations. The liquid energy equation can be written as:

$$\frac{\partial}{\partial t}\left[\bar{\rho}_l e_l\right] + \frac{\partial}{\partial x_j}\left[\bar{\rho}_l u_{l,j} e_l\right] = \dot{M}\left[L_{eff} - L - e_{ls}\right] \tag{13}$$

## 3. WAVE DYNAMICS

Equations (1), (5), and (12) can be re-stated together with Eq. (8) to form the basis for the development of a wave equation. The superscript bar is omitted here for convenience in further analysis.

$$\frac{\partial\rho}{\partial t} + \frac{\partial}{\partial x_j}\left(\rho u_j\right) = \dot{M} \qquad \frac{\partial}{\partial t}\left(\rho u_i\right) + \frac{\partial}{\partial x_j}\left(\rho u_j u_i\right) + \frac{\partial p}{\partial x_i} = \dot{I}_i$$
$$p = \rho RT \qquad \frac{\partial}{\partial t}(\rho h) + \frac{\partial}{\partial x_j}\left(\rho u_j h\right) - \frac{\partial p}{\partial x_j} - E \quad = \dot{\varepsilon} \tag{14}$$

The development of a wave equation begins by subtracting the divergence of the momentum equation from the time derivative of the continuity equation above. This yields

$$\frac{\partial^2\rho}{\partial t^2} - \frac{\partial^2 p}{\partial x_j \partial x_j} = \frac{\partial^2\left(\rho u_i u_j\right)}{\partial x_i \partial x_j} + \frac{\partial\dot{M}}{\partial t} - \frac{\partial\dot{I}_j}{\partial x_j} \tag{15}$$

Neglect of the variation of the gas constant $R$ due to the multicomponent nature of the fluid, assumption of constant specific heats $c_p$ and $c_v$ with $h = c_p T$ and $\gamma = c_p/c_v$, and differentiation of the perfect gas equation gives

$$\frac{\partial\rho}{\partial t} = \frac{\gamma}{a^2}\frac{\partial p}{\partial t} - \frac{(\gamma - 1)\,\rho}{a^2}\frac{\partial h}{\partial t} \tag{16}$$

Use of the combined First and Second Laws of Thermodynamics to write:

$$\rho \frac{\partial h}{\partial x_i} = \frac{\partial p}{\partial x_i} + \rho T \frac{\partial s}{\partial x_i}$$

and substitution for $\partial h/\partial x_i$ in the energy equation (12) using the continuity equation (1) leads to

$$\rho \frac{\partial h}{\partial t} = \frac{\partial p}{\partial t} - \rho u_j T \frac{\partial s}{\partial x_j} + E + \dot{\varepsilon} - h\dot{M} \tag{17}$$

Combine Eqs. (16) and (17) to eliminate enthalpy and differentiate again with respect to time to obtain a second derivative of density with respect to time. Eliminate by substitution that second derivative from Eq. (15). Note that, for a perfect gas, $(\gamma - 1)\, h = a^2$.

$$\frac{\partial^2 p}{\partial t^2} - a^2 \frac{\partial^2 p}{\partial x_j \partial x_j} = \frac{\partial \rho}{\partial t} \frac{\partial a^2}{\partial t} + a^2 \frac{\partial^2 \left(\rho u_j u_i\right)}{\partial x_i \partial x_j} + (\gamma - 1) \frac{\partial E}{\partial t} + S_3 \tag{18}$$

where the 3D source term $S_3$ is given by

$$S_3 \equiv (\gamma - 1) \left[ \frac{\partial \dot{\varepsilon}}{\partial t} - \dot{M} \frac{\partial h}{\partial t} - \frac{\partial \left(\rho T u_j \partial s / \partial x_j\right)}{\partial t} \right] - a^2 \frac{\partial \dot{I}_j}{\partial x_j} \tag{19}$$

This equation may be solved simultaneously with Eq. (5) to solve for pressure $p$ and velocity components $u_i$. Other inputs are needed for coupling with liquid phase behavior and energy release from combustion processes.

The left-hand side of Eq. (18) represents the wave operator in three dimensions. A mild nonlinearity appears through the coefficient $a^2$. The first and second terms on the right-hand side are strongly nonlinear terms that are conservative and do not drive or damp the oscillation. However, they will affect the wave shape. The third and fourth terms on the right represent the influence of the chemical energy conversion rate $E$, viscous and transport effects embedded in the rates $\dot{I}_i$ and $\dot{\varepsilon}$, impact of volume fraction $\theta$, and exchanges of mass, momentum, and energy between the phases embedded in the rates $\dot{M}$, $\dot{I}_i$, and $\dot{\varepsilon}$, respectively. These terms can be strong drivers or strong dampers of the nonlinear oscillation; consequently, they will be discussed further below.

Entropy gradients in the flow can be neglected for the purpose of developing a model equation. Thus, one term in the definition given by Eq. (19) can be neglected. One can assume that fine-scale mixing eliminates these entropy gradients. The length scales for transverse gradients of entropy, other scalar properties and vorticity are of the order of the injector diameter, the order of spacing between adjacent injectors, or smaller. These dimensions are smaller than the common wavelengths of oscillations in the combustion chamber. Also, these properties advect and diffuse but are not propagated by acoustic waves. Turbulent mixing will uniformize these quantities rapidly while acoustical pressure and velocity oscillations will not be vitiated by turbulence. These comments would not pertain to entropy generation if the acoustic waves form shock waves or detonations, which are possibilities for longitudinal oscillations and, in an annular chamber, for transverse oscillations. In that case, the entropy generation (i.e., shock dissipation) can be significant in determining the limit-cycle oscillation amplitude.

In evaluating driving and damping mechanisms for the wave equation (18), realize that a hypothetical first-time-derivative-of-pressure term appearing on the right side with a positive coefficient would be a driving term through which energy is added to the oscillation. With a negative coefficient on the right side, the term would provide damping for the oscillations. Consequently, the question is whether $E$, $\dot{M}$, and $\dot{\varepsilon}$ are in-phase or out-of-phase with the oscillating pressure. Thus, if the rate at which energy is added locally via oxidation or transport is in-phase (out-of-phase) with pressure, driving (damping) of the oscillation is occurring at that location. If the divergence of the impulse $I_i$ is in-phase (out-of-phase) with the pressure first time derivative, damping (driving) of the oscillation appears. "In-phase" or "out-of-phase" each implies a band so that phase angle can vary by $\pm 90°$.

Equation (18) is coupled with the velocity; thus, it should be solved simultaneously with Eq. (5). The system has higher derivatives appearing through the viscous and transport terms, which are included in source terms as presented. These higher derivatives create an elliptical system of equations if they are important terms. Typically, however, transport and viscosity manifest their impacts on a much smaller length scale than the acoustic wavelength. Therefore, the phenomenon remains hyperbolic rather than elliptical for practical purposes. One could set the viscous and transport terms to zero, yielding the following definitions of the inviscid sources $\varepsilon_I$ and $\dot{I}_{i,I}$:

$$\begin{aligned} \dot{\varepsilon}_I &\equiv (\theta - 1)\frac{dp}{dt} - \sum_k n^{(k)}\dot{m}^{(k)}L_{eff}^{(k)} + \sum_k n^{(k)}\dot{m}^{(k)}h_s^{(k)} \\ \dot{I}_{i,I} &\equiv (1-\theta)\frac{\partial p}{\partial x_i} + \sum_k n^{(k)}\dot{m}^{(k)}u_{l,i}^{(k)} - F_{Di} \end{aligned} \tag{20}$$

Equation (18) will still be coupled with Eq. (5) to solve for velocity and pressure; however, for consistency, the viscous terms in the momentum equation should be neglected to solve for the wave behavior on the scale of the acoustic wavelength (or equivalently on the scale of the combustion chamber size). The aerodynamic force per volume for the condensed phase $F_{Di}$ includes both lift and drag; exceptions are made to retain this term in the inviscid limit because it affects droplet motion and position. Equation (18) now is strictly in hyperbolic form. The input for $E$ can involve an analysis on a finer length scale, accounting for transport and viscous terms. For a single-phase flow, the system is much simpler with the source terms $\dot{M}$, $\dot{I}_{i,I}$, and $\dot{\varepsilon}_I$ becoming identically zero. Nevertheless, the terms giving the highest derivatives remain the same for both the single-phase equation and the two-phase equation, reflecting the similarity of the wave propagation in both cases.

In the above formulation of the equations for the wave dynamics, selected consideration of turbulence has been advocated. Under the assumption that turbulent length scales are small compared to acoustical wavelengths, the affect on the dynamics is neglected. For the shorter kinematic (i.e., entropy, temperature, and vorticity) waves, turbulence is assumed to help uniformize those quantities and reduce the importance of those waves. For the many flames that have shorter characteristic lengths, the impact of turbulence can be important and must be evaluated. For example, consider a combustion chamber with many injectors, each of a size scale that is much smaller than the chamber size. If mixing is fast and chemical kinetics is controlling, the effect of the small-scale turbulence is not too important. However, if mixing is rate controlling, the small scales of turbulence can be very important.

### 3.1. Models for Source Terms

There is a need to close the conservation equations by describing the various source terms that appear: $\dot{\omega}_m$, $\dot{M}$, $\dot{I}_i$, and $\dot{\varepsilon}$. The chemical kinetic rates in a high-temperature, high-pressure rocket environment are commonly much faster than mixing and vaporization rates. Thus, great accuracy in their determination is generally not required because they are not rate controlling and do not significantly affect time lags. For that reason, a one-step chemical reaction model often suffices. Westbrook and Dryer (1984) provides useful one-step models for $\dot{\omega}_m$ in the case of hydrocarbon oxidation. A typical rate law for burning a hydrocarbon $C_xH_y$ would be of the form $\dot{\omega}_{C_xH_y} = A\rho^{a+b-1}Y^a_{C_xH_y}Y^b_{O_2}\exp\left[-E_A/\left(R_uT\right)\right]$.

For the modeling of $\dot{M}$ for spray flows, knowledge of the droplet size distribution or average droplet size produced in the atomization process is needed; the vaporization rate and lifetime of the individual droplet will depend on its initial size and $\dot{M}$ at $\vec{x}$, $t$ will depend on the vaporization rates of the droplets in that neighborhood at that instant. Then, a vaporization model is needed for the slower vaporizing propellant, which is the hydrocarbon fuel in liquid-hydrocarbon/oxygen engines but becomes the liquid oxygen with hydrogen/oxygen engines. Pioneering works on the vaporization and burning fuel droplets are described by Godsave (1953), Spalding (1953), and Williams (1958, 1959, 1960, 1985). Generally, the early theory focused on the burning of isolated droplets with spherically symmetric, quasi-steady gas phase and steady liquid temperature. More recent models add the effects of transient liquid-phase heat transfer, which is typically the slowest process in droplet heating, and vaporization in high temperature environments (Sirignano, 2010), internal liquid circulation and convective liquid heating, and gas-film convective heat transfer. The most-often-used model having those attributes was developed by Abramzon and Sirignano (1989). An extension of that model to address multi-component fuels was developed by Continillo and Sirignano (1988). It is desirable to have extensions that would account for interactions of the droplets with neighboring droplets and with the smaller turbulent eddies. We know that these interactions modify Nusselt number, Sherwood number, and drag coefficient from the values for isolated droplets. Consequently, vaporization rates and drag forces are modified. Sirignano (2014) reviews recent progress in those directions. Related issues will be discussed in the next section.

### 3.2. Boundary Conditions

**Wall conditions.** Equation (4) shows that the total normal stress is zero at a wall where the normal velocity of each phase must go to zero. For the inviscid case, this means both normal velocity and normal pressure gradient are zero at the wall; tangential velocity may be non-zero. For the viscous case, normal velocity and normal pressure gradient can be set to zero also because normal viscous stress should be negligible; tangential velocity is also zero. If a wall has an acoustic liner, the admittance for that liner may be used as a boundary condition (Sirignano, 1972; Tang and Sirignano, 1973; Tang et al., 1973).

**Injector or burning surface.** For a liquid-propellant rocket engine, portions of an injector face will essentially be a wall with wall-type boundary conditions on the normal vectors. Other portions will be orifice exits where jet flows occur. Here, traditional inflow conditions can be placed on mass flow (or velocity), temperature, and composition. If mass inflow is controlled, the boundary conditions can be placed on mass flux with density and velocity allowed to adjust with pressure oscillation. If the injector experiences internal oscillations, a coupled analysis of injector and chamber flow might be needed with

boundary conditions set upstream at a plenum (Popov et al., 2014; Sirignano and Popov, 2013). At the gasifying surface of a solid propellant in a solid-propellant or hybrid rocket engine, the mass flux per unit area of the propellant (equal to the product of the regression rate and solid density) must be analyzed by coupling the gas-phase mixing and reaction layer with the solid-phase thermal layer (Krier et al., 1968; Sirignano, 1968).

**Choked nozzle flow.** The nozzle provides an important damping mechanism and modifier of natural frequencies. The nozzle has an acoustical impact between those of the open-end chamber and the closed-end chamber. Like the open-end, acoustical energy continually flows out. On the other hand, the convergent walls provide some reflection of waves. The modifications of effective chamber size by the addition of the convergent nozzle affects the natural resonant frequencies as well, generally reducing the magnitude as the nozzle volume increases.

Early work on the boundary condition at the entrance to the convergent choked nozzle for linear longitudinal-mode combustion-chamber oscillations was done by Tsien (1952) and Crocco and Cheng (1953, 1956). Extensions to 3D oscillations and nonlinear theory was performed by Crocco and co-workers (Crocco and Sirignano, 1967, 1966; Zinn and Crocco, 1968). The linear theory used admittance coefficients, which related pressure oscillations in the nozzle entrance plane to oscillations of velocity components and entropy (or temperature) at the same location. These coefficients were obtained by integration by Crocco and Sirignano (1967) of the equations governing the oscillations in the convergent portion of the nozzle. For a choked nozzle, acoustic signals will not propagate upstream from the throat; hence, the behavior of the flow in the divergent portion of the nozzle has no consequence on the chamber instability. In the limit of a short nozzle, the wavelength of the oscillation becomes much longer than the convergent length; thus, a quasi-steady nozzle flow can be assumed. For longitudinal oscillations, that means the chamber length is much greater than the convergent nozzle length and the Mach number at the nozzle entrance remains constant under oscillation although pressure and velocity fluctuate.

The short-nozzle boundary assumption applies for transverse-mode and 3D oscillations if the length of the convergent portion of the nozzle is of negligible length compared to both the chamber length and circumference and if the exit plane has many small closely-spaced equally sized and shaped nozzle holes so that the angle of convergence is not too large. Then, the relationship developed by Crocco and Sirignano (1966) applies. For isentropic nozzle flow of a perfect gas with constant specific heats,

$$\frac{1}{M_x}\left[1+\frac{\gamma-1}{2}\left(M_x^2+M_y^2\right)\right]^{(\gamma+1)2(\gamma-1)}=\left(\frac{\gamma+1}{2}\right)^{(\gamma+1)/2(\gamma-1)}\left(\frac{A_c}{A_t}\right) \tag{21}$$

where $a$ is the speed of sound at the entrance to the nozzle capture zone and the two components of Mach number at that entrance are $M_x = u/a$ and $M_y = v/a$. $A_c$ and $A_t$ are the nozzle flow capture area and throat area. The capture area is determined by following streamlines upstream for a short distance from the nozzle hole. The nozzle holes are considered to be sufficiently densely packed so that the nozzle entrance area and capture area differ only slightly. Furthermore, distances are sufficiently smaller than wavelengths so that quasi-steady flow is assumed and streamlines may be defined. For zero-valued transverse-velocity component (i.e., longitudinal-mode oscillation or steady state), $M_y = 0$ and therefore $M_x = u/a$ is constant, which provides a simple boundary condition. With a transverse component to the oscillation, both $M_x$ and $M_y$ can oscillate. Therefore, Eq. (21)

relates the two velocity components $u(t,L,Y)$ and $v(t,L,y)$ with the thermodynamic variable $a(t,L,y)$ at the chamber exit. Another form of the same relation is informative and is provided below:

$$\gamma^{1/2}\left[\frac{1+\left[(\gamma-1)/2\right]\left(M_x^2+M_y^2\right)}{(\gamma+1)/2}\right]^{(\gamma+1)/\left[2(\gamma-1)\right]}=\frac{A_c}{A_t}u\,(RT_c)^{-1/2}=\frac{\dot{m}\,(RT_c)^{1/2}}{A_t p_c} \quad (22)$$

where $\dot{m}$, $P_c$, and $T_c$ are the individual nozzle mass flux, capture-flow static pressure, and capture-flow static temperature. Note that the quantity on the far right side of Eq. (22) is constant for steady-state or longitudinal oscillations but $p_c$, $T_c$, and $\dot{m}$ may still oscillate there. Obviously, they can oscillate also for transverse modes where $M_x$ and $M_y$ also oscillate.

Using perturbation theory, Zinn and Crocco (1968) extended the use of 3D nozzle admittance coefficients to third order in a perturbation series of pressure amplitude.

## 4. MECHANISMS AND CHARACTERISTIC COMBUSTION TIMES

The combustion process generally responds to fluctuations and oscillations in density and temperature (which relate to pressure) and velocity. Gasification rates, mixing rates, and chemical rates can vary as these quantities fluctuate. Thereby, the rate $E$ in Eq. (18) depends upon the histories of the pressure $p$ and other variables. Consequently, an oscillation in $E$ might lag the oscillation in $p$. The classical Rayleigh criterion for optimal driving of the oscillation by the energy addition $E$ is met when $E$ and $p$ are exactly in phase (or equivalently when $E$ lags $p$ by a time equal to the period of oscillation multiplied by any positive integer). Some reduced amount of driving occurs when $E$ differs from one of the optimal lag values by less than one-quarter of the time period. The oscillation is damped when it lags by an amount that differs from every optimal value by more than one-quarter of the time period. Substantial analysis is required to determine the time lag associated with combustion under these oscillatory conditions.

Combustion can be viewed and well approximated as a sequence of processes for the reactants with each process coming to completion for a given infinitesimal element of mass before the next process: e.g., injection and atomization, vaporization, mixing, and exothermic chemical reaction. The overall time duration $\tau$ for $N$ sequential processes is the sum of the time durations of all processes. The rate $r$ of a process can be taken as the reciprocal of its duration. Thereby, the reciprocal of the overall rate $r_o$ becomes the sum of the reciprocal rates of the individual processes:

$$\tau=\sum_{i=1}^{N}\tau_i=\sum_{i=1}^{N}\frac{1}{r_i}=\frac{1}{r_o} \quad (23)$$

If one process $i=*$ becomes an order of magnitude larger in its duration than any other, we may approximate $r_o=r_*$; i.e., the slowest rate becomes controlling. Of course. if the overall duration $\tau$ of the combustion process becomes significant in magnitude compared to the period of oscillation, the combustion process is not quasi-steady and a history (i.e., time-lag) effect exists. The rate $E$ in Eq. (18) has units of energy per unit time per unit volume and differs from the $r_i$ values; however, the rate $E\left(t,\overrightarrow{x}\right)$ will depend on the values

of $r_i$ over the duration of the combustion process prior to time $t$ for the element of mass that completes combustion at time $t$ and point $\vec{x}$.

Combustion processes introduce many length and time scales. Those length scales generally are smaller than the acoustic wavelength and some of the flow structures. Some of the combustion time scales can be of the order of a wave travel time or period of oscillation. In the following subsections, the various descriptions of combustion processes are discussed. The Sensitive-Time-Lag approach was the early attempt to bypass a detailed description of combustion and is discussed first. The other subsections discuss specific combustion processes and their possible impacts on combustion instability.

### 4.1. Sensitive Time-Lag Theory

During the 1950s, when our knowledge of unsteady combustion processes was rather poor, Crocco and Cheng (1953) proposed the heuristic approach named the Sensitive Time-Lag Theory. Previously, a constant time lag had been used to explain the delayed response of injected liquid-propellant mass flux into a combustion chamber, which experienced a varying chamber pressure. The new theory differed because the time lag itself varied under oscillation of thermodynamic properties in the combustion chamber. In its first version, the combustion process rate was related only to pressure $p$.

The theory assumed that the energy release rate $E$ at time $t$ required a certain history prior to the instant of energy release at t; specifically, the pressure history had to satisfy the condition that the integral $\int_{t-\tau(t)}^{t} p\left(t'\right)^n dt' = C$ where $n$, $\tau$, and $C$ are, respectively, the constant (positive) interaction index, the instantaneous value of the time lag, and a constant independent of pressure. By a shortening (lengthening) of the time lag due to a positive (negative) pressure fluctuation, the mass burning rate became instantaneously faster (slower) than the injection rate of mass. The values of the interaction index and steady-state time lag f were intended to be determined empirically from choice of propellants and injector design.

Using perturbation theory, $p = \bar{p} + p'$, $\tau = \bar{\tau} + \tau'$ and $E = \bar{E} + E'$ linear theory shows that the time derivative of the time lag $d\tau/dt = d\tau'/dt = -n\left[p'(t) - p'(t-\bar{\tau})\right]$. Furthermore, it follows that:

$$\frac{\partial E}{\partial t} = \frac{\partial E'}{\partial t} = -\frac{\partial \tau}{\partial t} = -\frac{\partial \tau'}{\partial t} = n\left[p'(t) - p'(t-\bar{\tau})\right] \tag{24}$$

This presentation is somewhat simplified by the assumption that the mass undergoing the combustion process during the time lag does not change its position significantly during that duration. For a more general analysis, see Crocco and Cheng (1956). It can be seen that if the time lag $\bar{\tau}$ is the product of one-half the period of oscillation and an odd positive integer, the energy rate $E$ will be perfectly in phase with the pressure. If $\bar{\tau}$ differs by less than a quarter of an oscillation period from one of those optimal magnitudes, an in-phase component of $E$ will still be present supporting the oscillation in accordance with the Rayleigh criterion.

The theory met with some success in characterizing and predicting instability. For the transverse (i.e., 3D oscillation modes), the rate of combustion and subsequent time lag needed to be coupled with both pressure and gas velocity (Reardon et al., 1964). In the transverse oscillation, velocity had a stronger effect on atomization, vaporization, and mixing. The time-lag theory was extended to nonlinear analyses using a perturbation series

in amplitude (Crocco and Mitchell, 1969; Mitchell et al., 1969; Sirignano, 1964; Zinn, 1968). Zinn and Powell (1971) later used the time-lag theory with the Galerkin method for nonlinear oscillations.

The theory is strictly violated if, in order to match experimental data, $\bar{\tau}$ and/or $n$ must be considered as functions of the frequency of oscillation. This need to assume a frequency dependence has happened in some situations. A more general way to view the Sensitive Time-Lag Theory is as a two-parameter system where each of the parameters $n$, $\bar{\tau}$ can be functions of propellent selection, injector design, and oscillation frequency. Then, it becomes analogous to a gain-phase representation for the admittance $E'/p'$ as a complex number. In fact, $n$ and $\bar{\tau}$ can easily be related to gain, phase, and frequency. Others later legitimately used gain and phase for liquid-rocket instability analysis (Culick, 2006). As this author knows from personal communications, Professor Crocco viewed the Sensitive Time-Lag Theory (also known as the $n$, $\tau$ theory) as a heuristic attempt to analyze combustion instability until superior knowledge of unsteady combustion processes was developed.

### 4.2. Premixed Combustible Gaseous Propellants or Rapidly Mixed Propellants

In cases where the propellants are prevaporized and premixed before injection or rapidly mixed upon injection, the duration for the combustion processes can be very much shorter than the typical period of oscillation in a chamber. For example, the characteristic residence time for flow through a premixed flame can be $O(10^{-4} sec)$ while oscillation periods in combustors with dimensions of several tens of centimeters or greater will have periods of $O(10^{-3} sec)$ or larger. Thus, a reasonable approximation is that the rate $E$ responds to the instantaneous pressure or temperature without a lag. For the premixed flame, two rates enter Eq. (23): heating or mixing rate $r_M$ and chemical rate $r_R$. Since, in the quasi-steady flame, chemical rate determines heating rate in proportion, the overall rate (and the flame speed) becomes proportional to the square root of the product $r_M r_R$. This also determines the overall rate $E$. If the combustion zone is viewed as a well-stirred reactor where the mixing time is negligible and chemical kinetic rates are controlling, the chemical rate $r_R$ determines approximately the overall energy release rate per unit volume $E$.

These assumptions fit a certain experimental gas-rocket motor (Bowman, 1967; Bowman et al., 1965), which was analyzed using a nonlinear perturbation approach based on a 1D unsteady characteristic-coordinate method (Sirignano and Crocco, 1964). The results from experiment and theory agreed very well. That is, for combustible mixtures with high flame temperatures, the region with near-stoichiometric mixture ratio was stable while the lean and rich regions were unstable (see Figures 1 and 2). As the combustible mixture is diluted, the flame temperature lowers and the stability limits approach closer to the stoichiometric conditions for hydrogen fuel in Figure 1. For methane and air in Figure 2, the flame temperature is sufficiently low that the stoichiometric and near-stoichiometric region is unstable. However, enrichment of the air with oxygen yields higher flame temperatures and thus leads to separation into two zones of instability. In particular, one instability zone is for fuel-rich mixtures and the other is for fuel-lean mixtures with a stable zone near stoichiometric conditions. Periodic longitudinal-mode oscillations were observed with a shock wave traveling back and forth with reflections at the injector face and entrance to a short nozzle; near-sawtooth pressure profile oscillations were measured and predicted. The

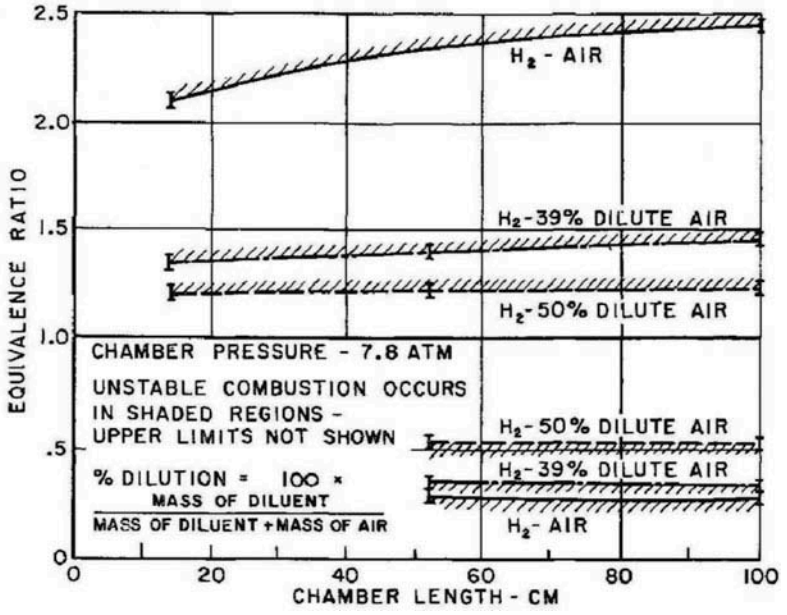


**Figure 1** Gas rocket instability domain as a function of chamber length and mixture ratio. (Reprinted from Bowman et al., 1965, with permission from AIAA)

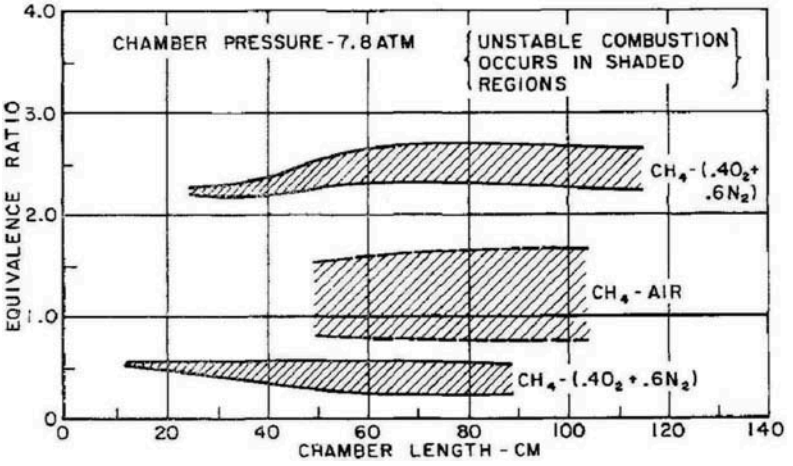


**Figure 2** Gas rocket instability domain as a function of chamber length and mixture ratio. (Reprinted from Bowman et al., 1965, with permission from AIAA)

amplitude of the oscillation was proportional to the mean-flow Mach number in the chamber at a fixed mixture ratio and grew as the mixture became more lean (for a lean mixture) or more rich (for a rich mixture). The flame temperatures at the rich and lean stability limits were identical at a value less than the stoichiometric adiabatic flame temperature.

The appearance of the identical value of temperature at both rich and lean was explained using a one-step chemical kinetic model by Sirignano and Crocco (1964). Their

theory used the inviscid equations in 1D form and considered only the single phase, i.e., gas. Therefore, $\theta = 1$, $\dot{\varepsilon} = 0$; $\dot{I}_i = 0$; $\dot{M} = 0$ in Eqs. (4) and (18). Using the characteristic coordinate form of the equations, it was possible to capture the discontinuous shock wave. Entropy waves were neglected and, since entropy jump across the shock is third order in pressure amplitude, that higher-order effect was neglected. If kinetics were rate controlling, $E \sim e^{-E_A R_u T}$, where $E_A$, $R_u$, and $T$ are the activation energy, universal gas constant, and flame temperature, respectively. From perturbation theory and the assumption of a polytropic relation between temperature and pressure (accurate to second order in amplitude), it follows that, for a well-stirred reactor model of the gas-rocket combustor,

$$E' \sim \frac{E_A T'}{R_u \bar{T} \bar{T}} e^{-E_A R_u \bar{T}} \sim \frac{E_A}{R_u \bar{T}} \bar{E} \frac{p'}{\bar{p}} \tag{25}$$

Therefore, for a given pressure perturbation, the fractional increase in burning rate $E'/\bar{E}$ becomes larger as the steady-state flame temperature $\bar{T}$ becomes smaller, i.e., as the mixture ratio moves further from the stoichiometric value in either direction. The mean burning rate $\bar{E} \sim M$ is the mean flow Mach number. Also, the nozzle admittance coefficient is proportional to $M$. Consequently, the nonlinear wave amplitude becomes proportional to $M$.

In this situation where the characteristic combustion time is negligibly small compared to the period of oscillation, the energy release rate $E$ is essentially instantaneously responsive to and in phase with the time-varying pressure $p$. Note that a very similar result appears with a quasi-steady premixed-flame model of the gas-rocket combustor. The only difference is that the square-root dependence makes $E_A/(2R_uT)$ replace the nondimensional factor $E_A/(R_uT)$, which appears in the well-stirred reactor model.

### 4.3. Mixing-Controlled Combustion

In some liquid-propellant rocket applications, the propellants are gaseous as they enter the combustion chamber. They might have been heated by prior use as a wall coolant as they flow towards the injectors. Or they might have flowed through a separate burner and been used to drive a turbo-pump before injection into the main combustor in a vitiated and heated form. Consequently, the two relevant rates are for mixing and exothermic chemical reaction, $r_M$ and $r_R$. A model for transverse combustion instability in this type of combustor has recently been created and used by Sirignano and Popov (2013) and Popov et al. (2014). The problem can be approached as a multi-scale problem.

On the scale of the wavelength, the wave dynamics can be considered as non-heat conducting, non-diffusive, and inviscid. Also, we have a single gaseous phase. Thus, $\theta = 1$, $\dot{\varepsilon} = 0$; $\dot{I}_i = 0$; $\dot{M} = 0$; in Eqs. (4) and (18). On the contrary, for the scale of the injector ports, which relate to the combustion scales, terms associated with viscosity, heat conduction, and mass diffusion were retained in the analysis of the flames. In particular, a separate analysis on a finer scale coupled Eqs. (1), (3), (5), and (12). That is, a turbulent, axisymmetric, transient jet-flame model was created for each injector to indicate spatial and temporal variations in temperature, species mass fractions, and chemical reaction rates in response to the local pressure oscillations. The value for $E$ in Eq. (18) was obtained from the $N$ jet-flame models for the $N$ co-axial injectors.

Figure 3 shows the magnitude of the in-phase response of $E'$ for one isolated co-axial methane-oxygen injector with imposition of a given amplitude magnitude of the sinusoidal

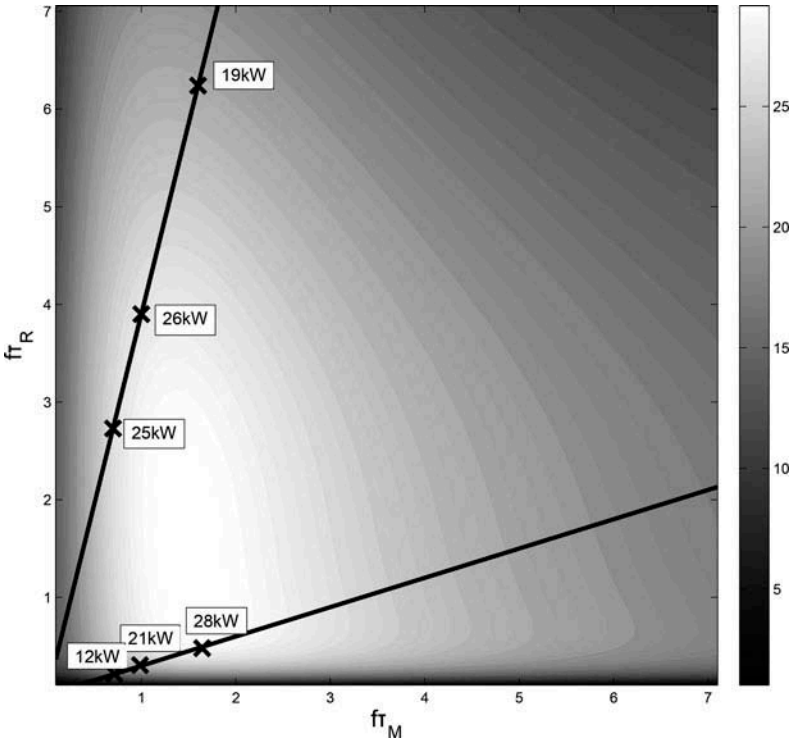


**Figure 3** Oscillation amplitude of in-phase component of $E$ for a given sinusoidal oscillation of $p$. The volume-integrated value of $E$ for an injector is presented in kilowatt units. [© William A. Sirignano. From Sirignano and Popov (2013). Reproduced by permission of William A. Sirignano. Permission to reuse must be obtained from the rightsholder.]

oscillation of $p'$. The contour plot shows the amplitude of the volume integral of $E$ contributed by that single coaxial methane-oxygen coaxial injector as a function of the two characteristic times normalized by the period of oscillation: $f\tau_M$ and $f\tau_R$ where $f$ is the oscillation frequency. Each straight line in the figure considers a fixed ratio of the characteristic combustion times, $\tau_M/\tau_R$ with varying $f$. The cross markings indicate locations of resonant transverse-mode oscillations for a given 28-cm-diameter, ten-injector combustion chamber. They correlate with regions of high response for $E$. One-step chemical kinetics and turbulent jet mixing models were used in the calculations by Sirignano and Popov (2013); the line slopes indicate that one path with the smaller slope has a longer mixing time while the other path with the steeper slope has a longer chemical time. Consequently, the first line corresponds to mixing-rate control while the other applies to kinetic-rate control. The oscillation of $E$ lags the pressure $p$ indicating that at least one of the characteristic combustion times is sufficiently long to produce the time-lag effect. The line with the lower value of the slope corresponds to actual experimental observations for methane oxidation. The case with the larger slope was artificially chosen to demonstrate the dependence.

At the high temperatures and pressures in the combustion chamber, the kinetics will be fast and mixing will become rate controlling. Turbulent diffusivities for heat and mass and a turbulent viscosity are chosen, which depend on the jet velocity at the exit of the injector and the injector radius. The jet velocity and, therefore, the diffusivities and

viscosity will oscillate with pressure in the two cases studied: (1) injector mass flux remains constant with pressure oscillation or (2) the flow through the injector is acoustically coupled to combustion chamber oscillation.

### 4.4. Vaporization-Controlled Combustion

In the case where liquid fuel (and/or liquid oxygen) is injected into the combustion chamber, two other characteristic combustion times are added. In addition to a gas mixing time and a chemical reaction time, a time for liquid stream breakup into droplets and a time for droplet vaporization are present. The atomization time is commonly of $O\left(10^{-5} - 10^{-4}\,\text{sec}\right)$, which means that it usually is fast enough compared to the oscillation period so that it can be taken as instantaneous. It usually is modified most from the nonoscillatory behavior by transverse velocity oscillations and changes would be in phase with that velocity. Thus, for a transverse spinning or traveling wave, the atomization process oscillation will be in phase with pressure while it is 90° out of phase for a tangential or radial standing mode. The fluctuation in the atomization process is very important because it affects the droplet-size distribution and, therefore, indirectly has substantial impact on combustion time lag.

For hydrocarbon fuels burning with oxygen or air, the vaporization time is commonly longer than the chemical time and mixing time. Therefore, it is rate controlling and determines the time lag in oscillatory combustion. Early works by Priem and Heidmann (1960) and Heidmann and Wieber (1965) considered implicitly a time lag in the heating of the liquid droplet interior, using a quasi-steady gas-phase assumption. However, they assumed that the temperature remained uniform through the liquid interior although time varying. This would increase the impact of the thermal inertia and underestimate fluctuations in surface temperature and vaporization rate during oscillation. In analyses by Strahle (1965a, 1965b, 1965c, 1967) and Williams (1965), the emphasis was placed on gas-phase unsteadiness while liquid-phase temperature did not oscillate. Flat-plate, stagnation-point, and wake-flame models were used. The examination of a time lag due to liquid heating with both spatial and temporal variations in the liquid-phase was first done by T'ien and Sirignano (1971) with the emphasis on the rocket combustion instability problem; a flat-plate model was used. The heating time of the liquid is the slowest process and, therefore, rate-controlling for the vaporization time. Consequently, the liquid-phase unsteadiness determines frequency range where vaporization rate is most responsive to fluctuations in the ambient gas. The most advanced droplet modeling is built on this premise (Sirignano, 2010).

For combustion instability cases where vaporization is rate controlling, the frequency domain where instability is most probable will align with the characteristic time for heating of the droplet liquid interior. (Exceptions can occur at high pressures in the near-critical domain, which is discussed in the next subsection.) One study of longitudinal-mode instability in a liquid-fueled ramjet combustor by Bhatia and Sirignano (1991) shows some interesting and relevant results for rockets as well as ramjets. They consider a 1D analysis of a combustion chamber at elevated pressure with inflowing decane droplets and air and a short, choked exit nozzle. Configurations with various chamber lengths, average initial droplet size, and mixture ratios were examined. Thereby, both the characteristic combustion time and the natural longitudinal frequency were varied widely. They used a vaporization model that accounted for transient heating of the droplet liquid interior and convective heating through a gas-film boundary layer and a liquid internal circulation due to relative

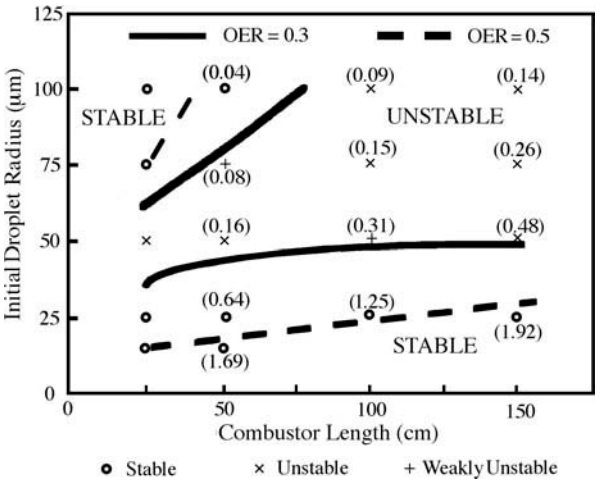


**Figure 4** Oscillation in spray combustor with choked nozzle. Stability limits for two overall equivalence ratios. Numbers in parentheses are ratios of oscillation period to droplet heating time. [© William A. Sirignano. From Bhatia and Sirignano (1991). Reproduced by permission of William A. Sirignano. Permission to reuse must be obtained from the rightsholder.]

gas-droplet motion (Abramzon and Sirignano, 1989). One-step chemical kinetics were used following Westbrook and Dryer (1984). The droplet vaporization time is controlled by the time to heat the liquid interior and in this way depends on initial droplet size. For vaporization control, we expect vaporization time and combustion time to vary with initial droplet radius to a power between one and two (Sirignano, 2010).

Figure 4 shows the correlation between oscillation frequency (or period) and characteristic combustion time lag. The unstable region centers around a certain range of time ratios. For the leaner mixture, the zone of instability becomes more narrow, which is expected because the energy per unit mass added to the gas through combustion decreases with equivalence ratio. Note that these results differ from the findings in subsection 4.2 since chemical-kinetic-rate control and mixing/vaporization-rate control produce different dependencies for the rate. For very small droplet size, the two results are expected to come closer, which is seen to some extent. As the droplet size becomes smaller, the combustion time lag becomes shorter and the instability limit depends less on the frequency (or equivalently the chamber length). Note that finding about frequency dependence is consistent with the experimental and theoretical results for the kinetics-controlled unstable combustor (Bowman et al., 1965; Sirignano and Crocco, 1964) where the limit became virtually independent of frequency. The time-ratio for maximum instability of about 0.15 is consistent with the calculations of Tong and Sirignano (1989) when adjustments are made for different normalization schemes.

There are various other physical phenomena with new time and length scales that can affect vaporization rates. Turbulence can interact with droplets. Smaller scales of turbulence can modify transport rates substantially through modification of Nusselt and Sherwood numbers. Larger scales of turbulence can modify ambient conditions and move droplets through drag forces. In a dense spray, transport properties can be significantly reduced from the values for an isolated droplet. These effects are reviewed by Sirignano (2014) and Sirignano (2010) and will not be discussed in detail here.

### 4.5. Transcritical and Supercritical Combustion

Development of aerospace propulsion engines is generally in the direction of increasing combustion chamber pressure. Thereby, injection and combustion of propellants at near-critical and supercritical thermodynamic conditions are relevant. There are key challenges associated with combustion at near-critical and supercritical conditions The distinction between liquids and gases disappears at high pressures above the thermodynamic critical point, which has a strong nonlinear dependence on the composition. This introduces some crucial phenomena that are neglected when the compositional distinction between the original liquid and its surrounding gases in the combustor were neglected. Also, the reduced surface tension can cause a new mechanism to be the rate-controlling factor for energy conversion. Introductions of the major scientific issues for transport and thermodynamics in this new combustor environment are given by Yang (2000), Zong and Yang (2006), Schmitt et al. (2011), Sirignano and Delplanque (1999), and Sirignano (2010).

Transitions in the propellant flow between subcritical conditions and supercritical conditions can occur in several ways. Two or more initially supercritical propellant flows might be mixed to yield a mixture that is subcritical at the same pressure. A flow initially at supercritical pressure but at subcritical temperature can be heated by combustion to achieve supercritical temperature. Propellant flows, which are initially at supercritical pressure, might be expanded to subcritical pressure. These situations can create transcritical behavior in a spatial sense and/or a temporal sense.

As a subcritical flow enters the near-critical domain, some interesting phenomena may occur. Decreasing and ultimately disappearing values of the coefficient of surface tension and the energy of vaporization must be considered. There is a need for accurate equations of state. Consequently, a more sophisticated analysis of the thermodynamics is required than is normally used for combustion and liquid injection at lower pressures. The rate-controlling mechanisms for combustion can change as the critical point is approached or exceeded. For example, at low surface tension values, the secondary atomization of "parent" droplets and vaporization of resulting smaller droplets might be faster than the vaporization rate of the parent droplet. Or the breakup of the injected stream could result in a very different distribution of droplet size. Another possibility is that, with reduced energy of vaporization, mixing of vapors with surrounding gas might be slower than the vaporization rate. Depending on the propellant combination, the role as the liquid propellant with the slower vaporization rate could change between fuel and oxidizer as the critical point for one of the propellants is approached. Thereby, it is necessary to consider a range of possible transitions, giving several interpretations to the description of transcritical behavior.

High-pressure and supercritical ambient conditions have a considerable influence on the mechanisms controlling engine behavior and performance. Most of these effects are related to droplet behavior. When liquid is injected into a combustion chamber that is filled with a gas at supercritical thermodynamic conditions, all aspects of the combustion process from atomization to chemical reaction can be expected to depart significantly from the better-known subcritical patterns. Many practical applications involve the introduction of the spray into an environment where the ambient pressure is supercritical for the liquid but the liquid starts with a subcritical temperature below the ambient gas temperature. In this case, there is a distinction between the phases in spite of the supercritical pressure; discontinuities in density and composition occur across the interface between the droplets in the spray and the surrounding gas. Typically, the ambient gas is a different species from the liquid. The case where the liquid is introduced into an environment that consists solely

of its own vapor is of very limited interest. Generally, heat is supplied from the higher temperature gas to vaporize the liquid. Heat transfer takes a finite, albeit very short, time. While the liquid is heating, some vaporization occurs. The liquid temperature at the interface can eventually rise to the critical temperature for the given pressure. Once that surface temperature reaches the critical value, there is a continuous variation of density and other properties across the "interface." Quotation marks are used because the lack of any discontinuity there removes its right to be called a true interface. Anyway, this "interface" becomes a surface along which the critical temperature exists with liquid on one side (for subcritical temperature) and the supercritical fluid on the other side. With time and continued heating, this surface propagates into the liquid until all of the liquid reaches a critical temperature.

Proper algorithms are needed to formulate computational models, including subgrid models, to address these transcritical situations where propellants or fuel pass through phase transitions related to the thermodynamic critical point. Models for vaporization of hydrocarbon fuels in an oxidizing gaseous environment have been developed by Hsiao et al. (2011), Zong and Yang (2006), and Hsieh et al. (1991). For oxygen droplets vaporizing in a hydrogen gas environment, see Delplanque and Sirignano (1993) and Yang and Lin (1994). Delplanque and Sirignano (1995) considered vaporization at transcritical conditions with droplets moving in a convective environment; Delplanque and Sirignano (1994) considered the effects of liquid stripping from the droplet surface at reduced surface tension. Delplanque and Sirignano (1996) analyzed these effects in an unstable combustor.

Consider a spherically symmetric, constant-pressure situation in which Fick's law governs mass diffusion. The gas solubility in the liquid becomes important near the critical point so that even if the liquid phase is initially monocomponent, it is necessary to consider multicomponent behavior in the liquid phase. The liquid density must also be considered as variable rather than constant. Therefore, the same unsteady forms of the continuity, species, and energy equations are used in both the liquid and the gas phases. Note, however, that the energy of vaporization will decrease as the critical point is approached; now, it must be considered to be strongly dependent on the thermodynamic state. The thermal, mechanical, and chemical equilibria at the interface are expressed by the continuity across the interface of the temperature, pressure, and chemical potential, respectively.

Typical models (Delplanque and Sirignano, 1993) include a detailed computation of the high-pressure phase equilibria based on a cubic equation of state. A prevalent cubic equation of state used in this range of pressures and temperatures by the spray combustion community has been the Redlich-Kwong equation of state:

$$p = \frac{RT}{(v-b)} - \frac{a}{T^{0.5} v\,(v+b)} \tag{26}$$

where $v$ is the specific volume. This empirical cubic equation has only two parameters, $a$ and $b$.

The enthalpy of vaporization to be used in the energy-balance condition at the interface is the energy per unit mass (or per mole if preferred) required for vaporizing at the given temperature and pressure and into the particular surrounding gaseous mixture. On the other hand, the latent heat used at conditions well below initial values is the energy per unit mass required for vaporizing the liquid into an environment composed of its own vapor. The enthalpy of vaporization for each species can be determined as a function of interface temperature, mole fractions on both sides of the interface, and the molecular weight.

Another challenging issue inherent in the simulation of transcritical-phase processes is the evaluation of transport properties. Some transport properties (e.g., thermal conductivity) are expected to diverge at the critical transition. To quantify this singular behavior, a given transport property is considered to be the sum of a low-density value, an excess value due to high-pressure effects, and a critical enhancement, including the singular effects at the critical transition. While these transport-property singularities are important to our understanding of critical phenomena, their macroscopic effects on droplet behavior in conditions relevant to actual processes (e.g., convective droplet heating and vaporization) might not be so pertinent.

The predictions of current models are qualitatively consistent. After the introduction of a droplet into a hot, supercritical, quiescent environment, it is heated by conduction, and its diameter increases because the liquid density decreases as the temperature rises. Density inside the droplet is nonuniform and internal circulatory liquid convection can occur under shear forces produced by relative gas-droplet motion. The droplet surface temperature rises until it reaches the computed critical mixture value. During this phase, the mixture composition on either side of the liquid-gas interface is imposed by the chemical equilibrium and mass diffusion that occurs in the droplet.

See Figure 5 from the analysis by Delplanque and Sirignano (1993), which relates to the vaporization in $LOX/H_2$ liquid-propellant rocket motors. It shows regimes with distinct phases for the oxygen liquid and hydrogen gas. $Pr$ is the pressure divided by the critical pressure for pure oxygen. At pressures above the critical pressure (e.g., $Pr = 2$ through 7 in the figure) but temperatures below the critical temperature (about 154 K), it is still possible to obtain a phase equilibrium with, of course, distinction between the phases. When the liquid exists with the ambient gas differing from the pure vapor of the liquid, some mass exchange occurs; the vapor of the liquid enters the gas phase and some of the gas molecules enter the liquid. This exchange becomes more important as the critical point is approached. The figure shows that as $Pr$ increases, the equilibrium has a decreasing fraction of oxygen and an increasing fraction of hydrogen in the liquid at the interface. That is, more hydrogen has dissolved. The temperature value above which the phases are no longer distinct will decrease with increasing pressure. The energy of vaporization is non-zero in this domain but decreases with increasing temperature until it reaches zero at the temperature value where phase distinction disappears. The figure shows that for $Pr = 1$ or less, the liquid is nearly pure oxygen while the gas at the liquid interface might have a significant fraction of the vapor from the liquid. The vapor fraction goes to unity as the liquid temperature goes to the saturation value. This saturation temperature increases with pressure, reaching the critical temperature as the critical pressure is reached. Above that critical temperature value, the distinction between phases is lost. In an unpublished work, Yang and co-workers have made similar calculations for liquid dodecane $C_{12}H_{26}$ surrounded by oxygen gas.

Consider a droplet of liquid component $A$ in gaseous component $B$ at pressure $p_a$. The liquid initial temperature is $T\hat{e}$ and the initial ambient temperature is $T_a > T_l$. For conditions well below the critical conditions, temperature varies continuously throughout the surrounding gas and liquid interior and is continuous across the liquid-gas interface. A negligible amount of the ambient gas dissolves in the liquid; composition and densities are discontinuous across the interface but piecewise continuous in the gas and in the liquid. As the critical conditions are approached, ambient gas dissolves in the liquid and the magnitudes of the interface discontinuities in density and in composition decrease. Still, the critical temperature and the critical composition do not occur at the same point in space

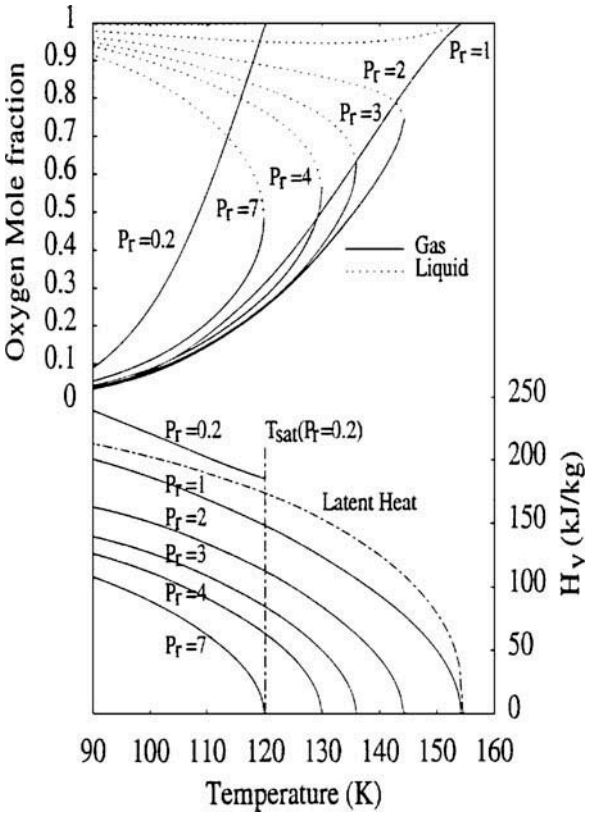


**Figure 5** Computed phase equilibrium of the oxygen/hydrogen system. [Reprinted from *International Journal of Heat and Mass Transfer*, vol. **36**(2), J.-P. Delplanque and W.A. Sirignano, "Numerical study of the transient vaporization of an oxygen droplet at sub- and super-critical conditions," pp. 303–314, 1993, with permission from Elsevier.]

and time. At the point when and where the discontinuity first disappears, the temperature, composition, and density assume their critical values simultaneously. After that time, the critical isotherm and the critical mass fraction isopleth must coincide. This critical surface that has replaced the interface will regress as further heating and mixture occur, until it reaches the droplet center. Therefore, the phenomena of mixing and vaporization can involve situations in which both a subcritical spacial domain and a supercritical spacial domain can exist simultaneously. This situation is described as transcritical.

Practical environments, such as those found in engines, are characterized by significant relative velocity between the gas and the droplet with subsequent strong convection. The first effect is that heat and mass transfer are enhanced by the convection. With near-critical and supercritical environments, the surface-tension coefficient of a droplet decreases to zero as the interface temperature approaches the critical conditions. Hence, the second effect is that droplet deformation and secondary atomization can be initiated by smaller values of the droplet-gas relative velocity. The aerodynamic consequence of droplet motion is that the fore and the aft pressures on the surface become greater than the pressures on the side. At reduced surface tension, there is a tendency therefore for the droplet to deform in an axisymmetric manner to the shape of a lens. The surface-tension force

will resist this deformation since it increases the surface area. For small values of Weber number $We = \rho_l U_s^2 L_s/\sigma_s$, and Bond number $Bo = a_s \rho_l L_s^2/\sigma_s$, there is some vibration but no significant deformation or breakup. $\rho_l$, $U_s$, $a_s$, $L_s$, and $\sigma_s$ are the liquid stream density, velocity, acceleration, characteristic length dimension, and surface tension, respectively. Above $We = 5$, aerodynamic forces have some effect on the droplet shape. A critical value of *We* occurs in the range 10–20, above which continuous deformation of the droplet occurs; the droplet has a convex side and a concave side and takes the shape of a bag or an umbrella. Viscosity does not play a significant role in this deformation. When *We* is above the critical value, the shear on the droplet surface will cause stripping of liquid from the surface. The critical value for the Bond number is 11.22 according to Harper et al. (1972); above that value, surface waves grow exponentially. The first unstable mode appears at and above $Bo = 11.22$. Other unstable modes will appear in sequence as *Bo* is continually increased. However, they remain small enough in magnitude until $Bo = O\left(10^4\right)$ so that the aerodynamic forces dominate. Experimental data for shock-wave interaction with a water droplet from Ranger and Nicholls (1972) indicates that stripping occurs above $Bo = 10^2$, filling the near wake with a mist.

Delplanque and Sirignano (1993) showed for droplet vaporization in a supercritical convective environment (with neglect of secondary atomization), based on the Abramzon and Sirignano (1989) film model, that a LOX droplet injected into a rocket engine is likely to reach the critical state before it disappears, much sooner than in a quiescent atmosphere. However, they showed that, because of the behavior of the surface-tension coefficient at near-critical conditions, a LOX droplet in a rocket engine is likely during its lifetime to undergo secondary atomization in the stripping regime (mass removal from its surface by aerodynamic shearing) before the droplet interface reaches the critical mixing conditions. Results obtained with this model confirmed that the stripping rate is much larger than the gasification rate. The predicted droplet lifetime was found to be reduced by at least one order of magnitude when stripping occurred. An important consequence is that, in most cases, the droplet disappears before the interface can reach the critical mixing conditions.

Now, it can be seen how this result can affect the predicted overall performance of propulsion systems and, in particular, the likelihood of combustion instability. The open-loop response of LOX droplets to prescribed oscillatory ambient conditions consistent with liquid rocket engines was investigated by Delplanque and Sirignano (1996) who used the supercritical droplet-combustion models described above both for isolated droplets and droplet arrays. This study evaluated the longitudinal-mode stability of the combustion chamber assuming concentrated combustion at the injector end, short nozzle, and isentropic flow downstream of the combustion zone, following the work of Crocco and Cheng (1956). A response factor *G* was computed to quantify the Rayleigh criterion, which states that an initially small-pressure perturbation will grow if the considered process adds energy in phase (or with a small enough phase lag) with pressure:

$$G = \iint \left(E' p'\right) \mathrm{d}t \, \mathrm{d}z \Big/ \iint \left(p'\right)^2 \mathrm{d}t \, \mathrm{d}z \tag{27}$$

The primes denote fluctuations with respect to the nonoscillatory values. Delplanque and Sirignano (1996) note that an underlying assumption to this definition of *G* is that the gasification rate provides a good approximation of the energy release rate *E*.

Figure 6 indicates that, at some frequency, the response factor, determined under the modeling assumptions by the droplet-gasification process, becomes large enough to drive

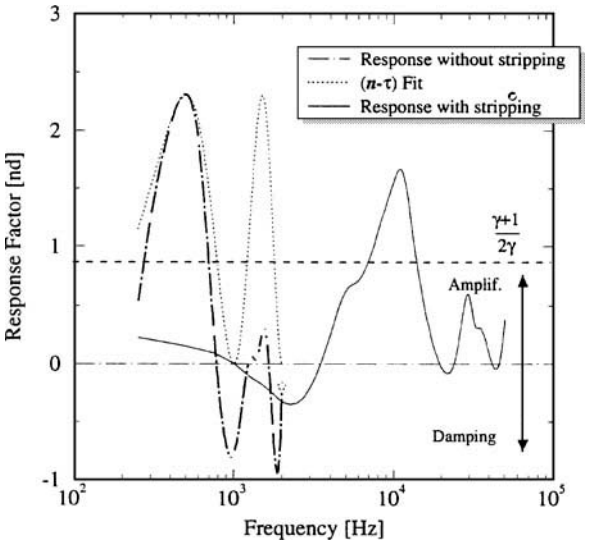


**Figure 6** Response factor for an isolated LOX droplet with and without stripping. $T_\infty = 1000$ K, $p_\infty = 100$ atm, $\Delta U = 20$ m/s. [© William A. Sirignano. From Delplanque and Sirignano (1996). Reproduced by permission of William A. Sirignano. Permission to reuse must be obtained from the rightsholder.]

longitudinal-mode combustion instability in a hydrogen-oxygen rocket engine. This conclusion applies whether the model includes droplet stripping or not. However, the unstable frequency domain for the stripping model is substantially higher. Obviously, the frequency at which the peak response factor occurs is mainly correlated to the droplet lifetime through the assumptions. Therefore, since secondary atomization in the stripping mode results in a reduction in droplet size and a one-order-of-magnitude reduction in droplet lifetime, it causes a substantial corresponding shift in the peak frequency, as shown in the figure. Consequently, when stripping occurs, the peak frequency is significantly larger than the acoustic frequencies of the common modes for standard cryogenic rocket engine chambers.

Delplanque and Sirignano (1996) argued that, since in these engines droplets with low surface tension are likely to undergo secondary atomization in the stripping regime for most of their lifetime, this phenomenon could explain the observed better stability of hydrogen/oxygen rocket engines compared with that of storable propellant engines (see Harrje and Reardon, 1972). Although their analysis applied strictly to the longitudinal mode, the qualitative implication for the transverse mode is even greater because both primary and secondary atomization processes with transverse modes could be more significant on droplet-size reductions.

Estimates by Delplanque and Sirignano (1996) of the influence of neighboring droplets on the droplet response to an oscillatory field obtained with the droplet-stream model described above indicate that the isolated droplet configuration underestimates the driving potential of the gasification process. In a dense spray, steady-state vaporization rate is reduced compared to vaporization rates in a dilute spray. Here, then, we have a situation similar qualitatively to the findings of the gas-rocket researches by Sirignano and Crocco (1964) and Bowman et al. (1965); instability is more likely as mean energy conversion rate is decreased. That is, the fractional increase in energy release rate for a given pressure perturbation increases as mean energy release rate decreases.

### 4.6. Solid-Propellant Burning

Although the emphasis in this article is on liquid fuels and propellants, brief mention can be made of time lags existing in solid propellant burning. The intent is to show the potential for fundamental similarities between solid burning, liquid burning, and the burning of gaseous propellants. While the condensed phase now is solid, it still possesses a characteristic time for heating. Commonly, gas-phase processes are more rapid and can be considered as unsteady. Models using an unsteady solid-phase heating coupled with a quasi-steady gas phase have been presented by Krier et al. (1968), Denison and Baum (1961), and Culick (1967). There have also been many approaches where a two-parameter model, e.g., gain and phase of response, has been used to represent combustion processes (Culick, 1976). These earlier models used a quasi-steady gas-phase model. Some more recent efforts treat more general conditions; for example, see Roh et al. (1995) and Jackson (2012) for models of homogeneous and heterogeneous propellant modeling, respectively.

The model of Krier et al. (1968) (KTSS) used an empirical correlation to relate the quasi-steady gas-flame behavior to the oscillating pressure. However, it allowed the solid surface temperature to fluctuate. Essentially, the pressure value primarily affected the heat flux from the flame back towards the solid-gas interface. The equation for unsteady heat diffusion in the solid was solved. With the frame of reference fixed to the regressing interface, a 1D convective-diffusive equation resulted. The regression rate was caused by temperature-dependent pyrolysis to give a closed system of equations. Sirignano (1968) used the KTSS model to describe longitudinal combustion instability in an end-burning solid rocket motor with a short (i.e., quasi-steady) nozzle. The fluctuating gaseous velocity at the solid surface was related via a history integral to the pressure fluctuation at the surface. Essentially, a time lag appeared implicitly in the formulation through a kernel in the history integral; the characteristic time for heat transfer in the solid was given by $\alpha\left(\bar{\dot{r}}\right)^2$ where $\alpha$ and $\bar{\dot{r}}$ are the solid-phase thermal diffusivity and average surface regression rate, respectively.

## 5. DETERMINATION OF LIMIT-CYCLE AMPLITUDE AND TRIGGERING THRESHOLD

It is interesting to examine what factors control the amplitude of the limit cycle and the magnitude of the triggering threshold. Here, "limit cycle" means the stable limit cycle, which is approached as time goes to positive infinity, while "triggering threshold" means the unstable limit cycle that is theoretically approached as time goes to negative infinity. Some older results from perturbation theory and some more modern results from computational fluid dynamics will be discussed. Longitudinal-mode and transverse-mode oscillations will be examined, with and without shock wave formation. We can examine both old results from perturbation theory and new results from computational fluid dynamics (CFD) methods. Fewer assumptions are required for CFD but those results are less powerful in identification of the key mechanisms and the parameter dependencies.

Our perturbation approaches follow the coordinate perturbation approach initiated by Henri Poincaré (Minorsky, 1962) and expanded by Lighthill and Kuo to the method now known as the PLK method or method of strained coordinates (Crocco, 1972; Kevorkian and Cole, 1996).

### 5.1. Nonlinear Shock Wave Oscillations

Consider the first cases with shock formation that were studied in the 1960s using perturbation theory. Sirignano and Crocco (1964) and Sirignano (1964) analyzed nonlinear longitudinal-mode rocket motor oscillations with combustion concentrated at the injector; no time lag or history effect in the combustion response; and a short, quasi-steady choked exit nozzle. Sirignano (1968) considered a longitudinal-mode oscillation for an end-burning solid-rocket motor with combustion concentrated at the solid-propellant surface; a history effect on the combustion response through a history integral reflecting the solid-phase heating process; and a short, quasi-steady choked exit nozzle. Longitudinal-mode rocket motor oscillations with combustion concentrated at the injector; a time lag in the combustion response; and a short, quasi-steady choked exit nozzle were examined by Mitchell et al. (1969). Two cases were studied by Crocco and Mitchell (1969): (i) longitudinal-mode rocket motor oscillations with combustion distributed arbitrarily through the combustor; a time lag in the combustion response through the use of the Sensitive Time-Lag Theory; and a short, quasi-steady choked exit nozzle and (ii) tangential-mode rocket motor oscillations in an annular combustor with combustion distributed arbitrarily through the combustor; a time lag in the combustion response through the use of the Sensitive Time-Lag Theory; and a multi-orifice exit with many short, quasi-steady choked nozzles.

These perturbation theories sought the limit-cycle behavior using first- and second-order perturbation. In accordance with typical analyses in nonlinear mechanics, the complete description of the first-order terms could only be obtained through examination of second-order terms. That is, the first-order result is very different from the result of linear perturbation theory. The nonlinear theory predicts a sawtooth wave profile for pressure with shock discontinuities while linear theory would predict continuous, sinusoidal waveforms. Linear theory cannot predict limit-cycle amplitude. A good estimate of amplitude and a more exact determination of frequency comes from the second-order theory. To first order, these above-cited longitudinal-mode nonlinear theories obtain first-order solutions for velocity perturbation $u_1$, speed-of-sound perturbation $a_1$, and pressure perturbation $p_1$ in the forms:

$$\begin{aligned} u_1 &= f(\theta - x) - f(\theta + x) \\ a_1 &= \frac{\gamma - 1}{2}\left[f(\theta - x) + f(\theta + x)\right] \\ p_1 &= \frac{\gamma \bar{p}}{\bar{a}}\left[f(\theta - x) + f(\theta + x)\right] \end{aligned} \tag{28}$$

where the function $f$ has velocity units, $\bar{p}$ and $\bar{a}$ are steady-state values for pressure and sound speed, $\theta$ is time normalized by one-half of the oscillation period, and $x$ is chamber axial position measured from the injector and normalized by chamber length $L$. The frequency and period of oscillation are not known a priori. Thus, the transformation to $\theta$ involves the introductions of a new strained coordinate and a perturbation series in an amplitude parameter for the period of oscillation. Thus, $0 \leq \theta \leq 2$ and $0 \leq x \leq 1$. For the transverse mode in the annular chamber, $x$ should be replaced by a nondimensional circumferential position $y$ and the axial velocity perturbation $u_1$ should be replaced by the tangential velocity perturbation $v_1$. Also, in that configuration, a traveling (spinning) wave represented by either $f(\theta - y)$ or $f(\theta + y)$ or the standing wave given by a sum of the

two functions can appear. The first-order analysis determines the forms given in Eq. (28); however, the determination of the specific function $f$ requires a second-order analysis.

The periodic function $f(\theta)$ is found in all of these cases to be governed by a differential equation of the following form:

$$\left[f - f_m\right] \frac{df}{d\theta} = -Af - Bf^2 + Cf^{\tau} + DF(f) \equiv H(f) \tag{29}$$

$$f_m \equiv \frac{1}{2}\left[f(0) + f(2)\right] \quad f^{\tau} \equiv f(\theta - \tau) \quad \int_0^2 f\left(\theta'\right) d\theta' = 0 \tag{30}$$

where $A$, $B$, $C$, and $D$ are positive constants and the functional $F(f)$ is an integral of $f$. Sirignano and Crocco (1964) had $C = D = 0$, i.e., no time lag or integral and $B << A$. With $B = 0$, the median value at the shock $f_m = 0$ and the solution for $f(\theta)$ is a linear function with identical discontinuities at 0 and 2 reflecting the periodicity. With a small value of $B$, mild exponential curvature occurs between the discontinuities but the shape is still essentially a "sawtooth" form. Sirignano (1968) had $B = C = 0$ with a history integral $F(f) = \int_{-\infty}^{\theta} v\left(\theta - \theta'\right) f\left(\theta'\right) d\theta'$ where $v$ is the kernel resulting from solution of the diffusive-convective equation in the solid propellant. Mitchell et al. (1969) had $B = D = 0$ while Crocco and Mitchell (1969) had $B = 0$ with the functional $F(f)$ appearing as a (1D) volume integral of combustion sources.

The left side of Eq. (29) results only from the nonlinear gasdynamics description of the chamber flow; combustion processes and nozzle boundary conditions do not affect it. Of the four terms on the right side of the first equality in Eq. (29), the last three result only from the coupling with the combustion process. A portion of the first term can also come from the combustion process while the remainder of the first term is the effect of the nozzle boundary condition. The details behind the modeling and the determination of the particular values of the coefficients $A$, $B$, $C$, and $D$ can be found in the four references cited in the previous paragraph. The Mach number at the entrance of the short nozzle remains constant; thereby, the velocity perturbation remains proportional to the sound-speed perturbation, giving a linear term in the function $f$. The combustion source terms also appear to linear order albeit in the second-order balancing of terms. The combustion terms appear representing velocity fluctuations at the injector end for combustion concentrated there. For the distributed combustion case, they appear representing fluctuations in the divergence of the velocity throughout the combustor volume. Note that the time-lag effect caused an infinite slope in $f$ (albeit with a continuous variation) at one value of the argument (other than the shock at $\theta = 0$ or 2) when $\bar{\tau}$ differed from one-half of the oscillation period (Mitchell et al., 1969). The history integral produces smoother profiles (Sirignano, 1968) and is more acceptable on physical grounds.

The linear stability limit is defined by neglecting the nonlinear terms on the left side of Eq. (29) and setting the left side to zero. At the stability limit, the amplitude of the oscillation goes to zero. At the stability limit, driving terms from combustion are exactly in balance with the nozzle damping. With displacement in parameter space from the stability limit, the amplitude becomes finite and is determined by the solution of the full nonlinear equation. Therefore, away from the stability limit, there is an imbalance between the combustion driving terms and the nozzle damping terms. When the former exceeds the latter, a finite-amplitude oscillation results; the left side of Eq. (29) represents that imbalance.

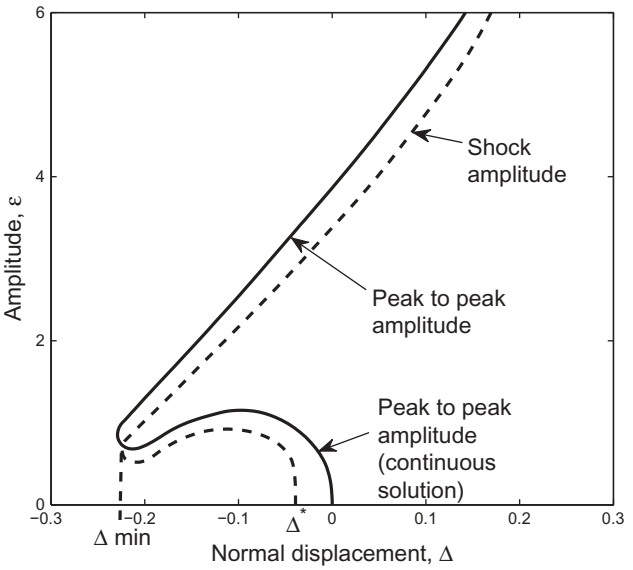


**Figure 7** Amplitudes for limit cycle and triggering threshold for longitudinal-mode analysis with shock waves using the **n**, $\tau$ theory. (Reprinted with the permission of Taylor & Francis from Mitchell et al., 1969.)

In the case where $C = D = 0$, Sirignano and Crocco (1964) obtained analytical solutions to Eq. (29). Numerical solution is required if the time lag, time history integral, or spacial integral appears. Figure 7 from Mitchell et al. (1969) shows amplitude as a function of normal displacement in **n**, $\tau$ parameter space from the linear stability limit. The curves result from the numerical solution of Eq. (29) for $B = D = 0$. Three domains exist: unconditionally unstable (right of linear stability limit); conditionally stable or bi-stable (near left of linear stability limit); and unconditionally stable (far left). In the conditionally stable region, two solutions are found; the lower amplitude describes the unstable limit cycle, which can be regarded as the triggering threshold. Disturbances of lower amplitude decay while larger disturbances will grow to the upper value, which describes the stable limit cycle. The stable limit cycle and a portion of the unstable limit cycle are solutions with shock waves. The region near the linear stability limit gives continuous solutions that are consistent with the results of Sirignano (1964). Any disturbance with amplitude lower than the limit-cycle amplitude will grow in the unconditionally unstable region. Amplitudes larger than the limit-cycle value will decay to that value but no more. All disturbances will decay in the unconditionally stable region.

There are several conclusions that are obvious from the above-described analysis. (i) Equation (29) has the same form and can use the same general numerical procedure for solution whether or not time-lag or history integrals are included. (ii) The results of Mitchell et al. (1969) as shown in Figure 7 and Crocco and Mitchell (1969) clearly demonstrate the solution also includes a stable limit cycle whenever an unstable limit cycle is produced. A stable limit cycle occurs in unconditionally unstable domains without the appearance of an unstable limit cycle but unstable limit cycles never appeared alone in those studies. (iii) Those studies from Mitchell's dissertation also predicted, as shown in the figure, a continuous parabolic portion of the unstable limit cycle that matches the description given by Sirignano (1964) and Zinn (1968). Note that these three points are totally misrepresented

in Chapter 7 of Culick (2006), which does well describing literature of the 1970s and later but poorly describing the pioneering work of the 1960s on nonlinear combustion instability. The misunderstanding about Point (ii) was sustained by Wicker et al. (1996).

Integration of Eq. (29) over the oscillation period yields the first equality below:

$$\frac{1}{2}\left[(f(2)-f_m)^2-(f(0)-f_m)^2\right]=\int_0^2 H(f)\,d\theta=0 \tag{31}$$

The second equality results because the magnitudes of $f(2)-f_m$ and $f(0)-f_m$ are identical although their signs are opposite. Now, multiply Eq. (29) by the quantity $f(\theta)-f_m+f_m$ and integrate over the period. Using the results of Eq. (31), it follows that:

$$\frac{1}{3}\left[(f(2)-f_m)^3-(f(0)-f_m)^3\right]=\int_0^2 f\,H(f)\,d\theta$$

or

$$\frac{2}{3}(f(0)-f_m)^3=-\int_0^2 f\,H(f)\,d\theta=\int_0^2\left[Af^2+Bf^3-Cf f^{\tau}-Df\,F(f)\right]d\theta \tag{32}$$

A new result can be shown through the use of Eq. (32). In particular, the right side of that equation can be shown to be proportional to the acoustic forcing per cycle from the combination of combustion and nozzle outflow while the left side can be shown to be proportional to the energy dissipation per cycle in the shock wave. This is a remarkable result because the original second-order analysis maintained isentropic flow through the shock; i.e., entropy gain is proportional to the cube of pressure change or velocity change across the shock and thereby third order in the the perturbation series. This result is consistent with a finding by Crocco (1972) that the power required to drive at resonance a piston at one end of a closed tube (filled with an inviscid compressible gas) balances the dissipation rate due to the shock wave.

As noted by Liepmann and Roshko (1957), the entropy change $\Delta s$ across a shock is of third order in terms of the pressure jump $\Delta p$ and is approximated by:

$$\frac{\Delta s}{R}\approx\frac{\gamma+1}{12\gamma^2}\left[\frac{\Delta p}{\bar{p}}\right]^3 \tag{33}$$

Note that within the accuracy of the approximation, it is allowed to substitute the mean pressure for the pressure in front of the shock. The pressure jump $\Delta p\approx\gamma\bar{p}\left[f(0)-f(2)\right]/\bar{a}=2\gamma\bar{p}\left[f(0)-f_m\right]/\bar{a}$. Therefore, the energy dissipation through the shock occurs at the rate $\rho U_s T\Delta s\approx\left[2\gamma(\gamma+1)\bar{p}/\left(3\bar{a}^2\right)\right]\left[f(0)-f_m\right]^3$, where within the accepted error the shock speed $U_s$ is taken as $\bar{a}$. The energy dissipated by the shock over a cycle is then $\left[4L\gamma(\gamma+1)\bar{p}/\left(3\bar{a}^3\right)\right]\left[f(0)-f_m\right]^3$. Neglecting higher-order terms in $M$, the period of the cycle is $2L/\bar{a}$.

The velocity at the nozzle entrance will be of the order of the mean-flow Mach number $M$. Thereby, the velocity and pressure fluctuations at the nozzle entrance are $u_1=0$; $u_2=Ma_1=\left[(\gamma-1)/2\right]M\left[f(\theta-1)+f(\theta+1)\right]$; and $p_1=\left[\gamma\bar{p}/(\bar{a})\right]\left[f(\theta-1)+f(\theta+1)\right]$. The product of $p_1$ and $u_2$ here gives the acoustic energy flux per unit area (Culick, 2006) at the nozzle. A positive amount implies that

energy is flowing out of the chamber. The integral of the product over a cycle yields $2ML\gamma\,(\gamma-1)\left[\bar{p}/\bar{a}^2\right]\int_0^2 f\,(\theta)^2\,d\theta$.

For the concentrated combustion at the injector end (or end-burning solid surface), the right side of Eq. (29) is

$$H\,(f)\equiv -Af-Bf^2+Cf^{\tau}+DF\,(f)=\frac{u_2\,|_{nozzle}-u_2|_{flame}}{\gamma+1}=O\,(M) \tag{34}$$

Now, the pressure fluctuation is identical (except for phase) at the two ends. So, multiplication by the pressure fluctuation $p_1$ at the injector end followed by integration over the period **T** of the cycle yields:

$$2\gamma\,(\gamma+1)\left(L\bar{p}/\bar{a}^2\right)\int_0^2 f\,(\theta)\,H\,(f\,(\theta))\,d\theta=\int_0^T\left[p_1u_2\,|_{nozzle}-p_1u_2|_{flame}\right]dt \tag{35}$$

Thus, multiplication of both sides of Eq. (32) by the factor $2\gamma\,(\gamma+1)\left(L\bar{p}/\bar{a}^2\right)$ results in a new equation with the dissipated energy by the shock over the cycle on the left side and the net acoustic flux integrated over a cycle on the right side of the equation. Consequently, when acoustic flux due to combustion adds energy to the chamber volume at a rate greater than the nozzle efflux, the difference is dissipated in the shock wave in order to establish a limit cycle. Essentially, Eq. (32) determines the amplitude of the limit cycle at an amount that maintains the necessary balance between the acoustic influx and the shock dissipation. While we have considered acoustic energy addition or subtraction only at the ends of the combustor, a double integration over the combustor volume and over the cycle time of the product of the pressure fluctuation with the combustion-driven divergence of the velocity fluctuation can also be added into this energy balance.

Realize that the coefficients *A, B, C,* and *D* in Eq. (29) are each $O(M)$ while $f$ itself is of the order of the amplitude of the fluctuation. That amplitude can be considered to be $O\,(\epsilon)$. Therefore, the left side of the equation, which is quadratic, is $O\left(\epsilon^2\right)$ while the right side, which is primarily linear, is $O\,(\epsilon M)$. The balance implies that at the limit cycle, a distinguished limit is established and the amplitude parameter $\epsilon=M$. This result is consistent with the analysis of Sirignano and Crocco (1964) and the experiments of Bowman et al. (1965).

### 5.2. Nonlinear Continuous Wave Oscillations

Continuous nonlinear wave oscillations were studied by Sirignano (1964) for the longitudinal mode and Zinn (1968) for the transverse modes. Both works at Princeton used the **n**, $\tau$ theory and concentrated combustion at the injector end. Each analysis required a perturbation series up through third order in the amplitude parameter $\epsilon$ in order to approximate the limit-cycle amplitude. Let us examine the need for a higher-order analysis than required for cases with shock waves. The character of the major results are shown in Figure 8.

The linear unstable domain is shaded in the upper sub-figures. The lowest value of **n** on the stability limit occurs with a time lag equal to one half of the period of oscillation. There, the negative sign in front of the lagged term of Eq. (24) means that both the instantaneous term and lagged term for energy addition are in phase with the pressure. Some portions of the linear stability limit curve are adjacent to conditionally stable domains (lower left sub-figure) while other portions are immediately adjacent to

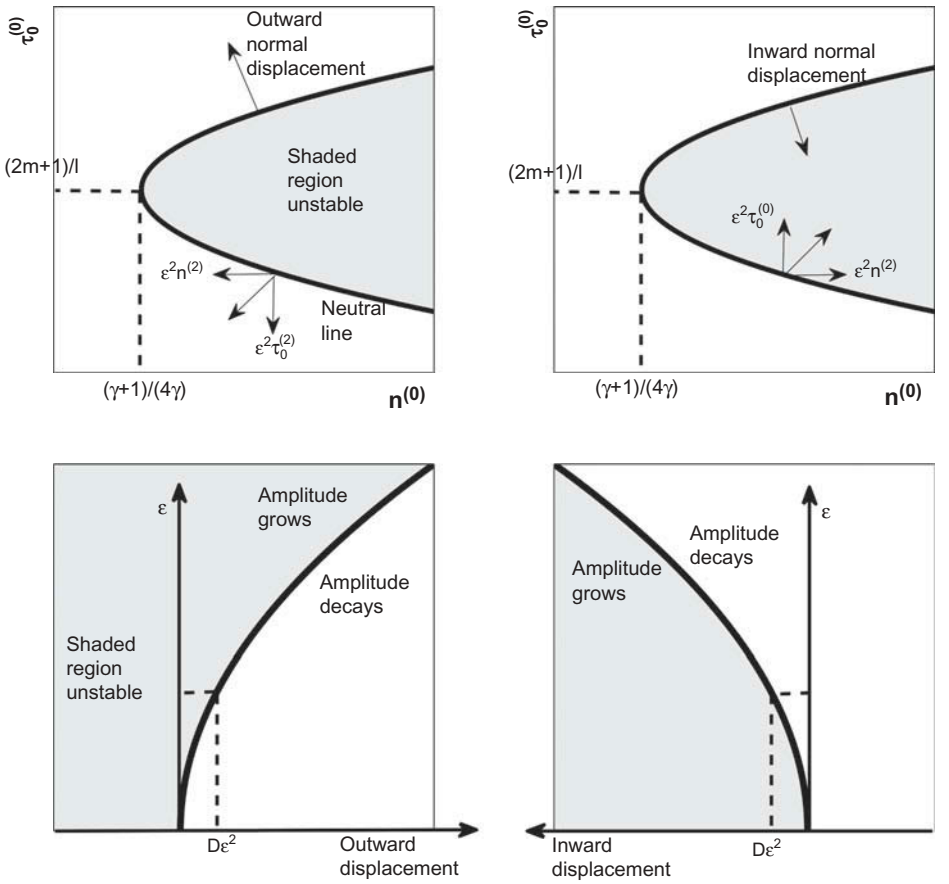


**Figure 8** Schematic of perturbation results in **n**, $\tau$. [© William A. Sirignano. From Sirignano and Popov (2013). Reproduced by permission of William A. Sirignano. Permission to reuse must be obtained from the rightsholder.]

unconditionally stable domains (lower right sub-figure). On the lower left, the unstable limit cycle (triggering threshold) is shown, while on the lower right a stable limit cycle is shown. Both curves are parabolas. That is, the amplitude parameter $\varepsilon$ grows as the square root of the normal displacement from the linear stability limit in the **n**, $\tau$ plane. Essentially, the development through third order in the perturbation series was needed to obtained the parabolic curves. These two analyses predicted either a stable limit cycle or an unstable limit cycle in the neighborhood of any point on the linear stability curve in parameter space. The expected higher-amplitude, stable limit cycle that accompanies a lower-amplitude, unstable limit cycle is not predicted with a third-order analysis. Presumably, a higher-order analysis would have predicted the two amplitude solutions in the conditionally stable domain; however, the perturbation expansions of both Sirignano (1964) and Zinn (1968) terminated at third order. Note the reassuring result though about the agreement among Mitchell et al. (1969), Sirignano, and Zinn about the parabolic shape of the nonlinear curve describing a continuous limit cycle. There are certain implications of these perturbation analyses that have not yet been discussed. We will return to this point later in this subsection.

Let us first examine some recent CFD results, which will complete the understanding of triggered transverse-mode combustion instability. In particular, we will focus on

transverse instabilities in a combustion chamber with gaseous propellants following the analysis of Sirignano and Popov (2013). The chamber exit is a multi-orifice plate with many short, choked nozzles. The work has been extended by Popov et al. (2014) to quantify the uncertainty with the triggering event in practical combustors. A 2D model is developed by integrating Eqs. (18) and (5) over the primary flow direction, $x_3$, after modification for an inviscid flow with gaseous propellants. A cylindrical combustion chamber is considered with the injector at $x_3 = 0$ and the nozzle entrance at $x_3 = L$. Variations of the pressure, velocity, and other variables in the $x_3$ direction will be smaller than variations in other directions.

Define the 2D average values: $\tilde{p} = (1/L)\int_0^L p dx_3$, $\tilde{\rho} = (1/L)\int_0^L \rho dx_3$, $\tilde{a} = (1/L)\int_0^L a dx_3$, and $\tilde{\vec{u}} = (1/L)\int_0^L \vec{u} dx_3$. Now, Eq. (18) is integrated over $x_3$, neglecting the difference between products of averages and averages of products. The pressure variation in the $x_3$ direction may be assumed to be minor for many transverse oscillations. The major variation of pressure will be in the transverse direction, as indicated by experimental findings of Harrje and Reardon (1972) and theoretical results of Reardon et al. (1964) and Zinn (1968). For a pure transverse wave behavior, there is not any acoustical oscillation in the $x_3$ direction; so, only advection can be expected to produce variations in that flow direction. These variations tend to be slow exponential variations according to the theory. Then, $p_{x_3=0} \approx p_{x_3=L} \approx \tilde{p}$. The average designation (i.e., superscript tilde) for pressure can be eliminated; we set $\tilde{p} = p$. The average designation is also removed for other variables. Entropy waves and other kinematic waves are neglected.

The 2D wave equation should be recast in cylindrical polar coordinates because of the combustion chamber shape. $r$ and $\theta$ will represent radial distance from the chamber centerline and azimuthal position, respectively. The pressure and velocity are normalized by the steady-state pressure and sound speed, respectively. The velocity components are $u_r$ and $u_\theta$. The resulting equations may be written as:

$$\frac{\partial^2 p}{\partial t^2} - C_1\left[\frac{\partial^2 p}{\partial r^2} + \frac{1}{r}\frac{\partial p}{\partial r} + \frac{1}{r^2}\frac{\partial^2 p}{\partial \theta^2}\right] = R\left(p, u_r, u_\theta\right) + S\left(p, u_r, u_\theta\right) \tag{36}$$

$$R\left(p, u_r, u_\theta\right) \equiv (\gamma - 1)\frac{\partial E}{\partial t} - A p^{\frac{\gamma-1}{2\gamma}}\frac{\partial p}{\partial t} \tag{37}$$

$$\begin{aligned} S\left(p, u_r, u_\theta\right) \equiv{}& C_1\left[p^{\frac{\gamma-1}{\gamma}} - 1\right]\left[\frac{\partial^2 p}{\partial r^2} + \frac{1}{r}\frac{\partial p}{\partial r} + \frac{1}{r^2}\frac{\partial^2 p}{\partial \theta^2}\right] + \frac{(\gamma-1)}{\gamma}\frac{1}{p}\left(\frac{\partial p}{\partial t}\right)^2 \\ &+ \gamma p^{\frac{\gamma-1}{\gamma}}\left[\frac{\partial^2\left(p^{\frac{1}{\gamma}}u_r^2\right)}{\partial r^2} + \frac{2}{r}\frac{\partial\left(p^{\frac{1}{\gamma}}u_r^2\right)}{\partial r} + \frac{2}{r}\frac{\partial^2\left(p^{\frac{1}{\gamma}}u_r u_\theta\right)}{\partial r \partial\theta}\right. \\ &\left. + \frac{2}{r^2}\frac{\partial\left(p^{\frac{1}{\gamma}}u_r u_\theta\right)}{\partial\theta} + \frac{1}{r^2}\frac{\partial^2\left(p^{\frac{1}{\gamma}}u_\theta^2\right)}{\partial\theta^2} - \frac{1}{r}\frac{\partial\left(p^{\frac{1}{\gamma}}u_\theta^2\right)}{\partial r}\right] \end{aligned} \tag{38}$$

$$\frac{\partial u_r}{\partial t} + C_2\frac{\partial p}{\partial r} = -u_r\frac{\partial u_r}{\partial r} - u_\theta\frac{1}{r}\frac{\partial u_r}{\partial\theta} + \frac{u_\theta^2}{r} + C_2\left[1 - \frac{1}{p^{\frac{1}{\gamma}}}\right]\frac{\partial p}{\partial r} \tag{39}$$

$$\frac{\partial u_\theta}{\partial t} + \frac{C_2}{r}\frac{\partial p}{\partial \theta} = -u_r \frac{\partial u_\theta}{\partial r} - u_\theta \frac{1}{r}\frac{\partial u_\theta}{\partial \theta} - \frac{u_r u_\theta}{r} + \frac{C_2}{r}\left[1 - \frac{1}{p^{\frac{1}{\gamma}}}\right]\frac{\partial p}{\partial \theta} \tag{40}$$

In the above equations, no acoustic coupling with the injection system has been considered. The model of coaxial injection, turbulent mixing, and chemical reaction discussed earlier in subsection 4.3 has been used to couple the above equations for the wave dynamics with the jet flame at the exit of each injector port. This model introduces physics and chemistry with characteristic times that will not be short compared to the period of acoustic oscillation. Therefore, time delays and a history effect are introduced. Consider a solid circular wall at radius $r = R$; that is, no acoustic lining is present. The normal velocity at the wall will be zero; thus, the following boundary conditions apply to the system of Eqs. (36), (39), and (40):

$$u_r(t, R, \theta) = 0 \qquad \frac{\partial p}{\partial r}(t, R, \theta) = \frac{p^{\frac{1}{\gamma}} u_\theta^2}{C_3 R} \tag{41}$$

$C_1$, $C_2$, and $C_3$ are known constants.

Typical results from a calculation of Sirignano and Popov (2013) and Popov et al. (2014) are shown in Figure 9. The initial amplitude of a disturbance is shown by the hollow circles while the black circles indicate the amplitude after 12 cycles of oscillation. Below the threshold disturbance of 20 atm, the disturbance decays in time towards the steady state. Above that threshold, it grows towards a limit-cycle amplitude of 154 atm. Near the threshold, the growth or decay is slower; sample calculations up to 120 cycles show the same outcome though. Clearly, the operating conditions (mean-flow Mach number, mean chamber pressure, mixture ratio) for this case place it within a conditionally stable (bistable) domain. When operating conditions are modified sufficiently in certain directions both unconditionally unstable and unconditionally stable domains are found immediately adjacent in parameter space, a qualitatively similar situation to the portrait of Figure 7. However, in this case, no shock waves resulted. Depending on the operating conditions and the nature of the triggering disturbance, either traveling (spinning) waves or standing waves could occur. The traveling wave shapes limit cycles found could be composed of a basic resonant mode plus superimposed harmonics of that mode. In that case, the pressure wave shape did not wobble but was reasonably steady in a certain rotating frame of reference. Note that, for transverse oscillations, the resonant mode frequencies are not integer multiples of the fundamental resonant mode (unlike the longitudinal mode situation). This explains why shock waves are unlikely to form in transverse mode oscillations in a circular cylinder. (Annular chambers can cause exception here.) A second type of limit cycle found in these computations for other operating conditions could involve the superposition of several resonant modes. In fact, in one case, a subharmonic mode was added with a frequency equal to the difference between the frequencies of the first and second tangential modes, which were also present. In this second type of situation, the superimposed frequencies are not commensurate and a temporally wobbly pressure waveform is observed in any rotating frame.

The results of Sirignano and Popov (2013) and Popov et al. (2014) identify several difficulties with a Galerkin method or any reduced basis method that identifies a priori the

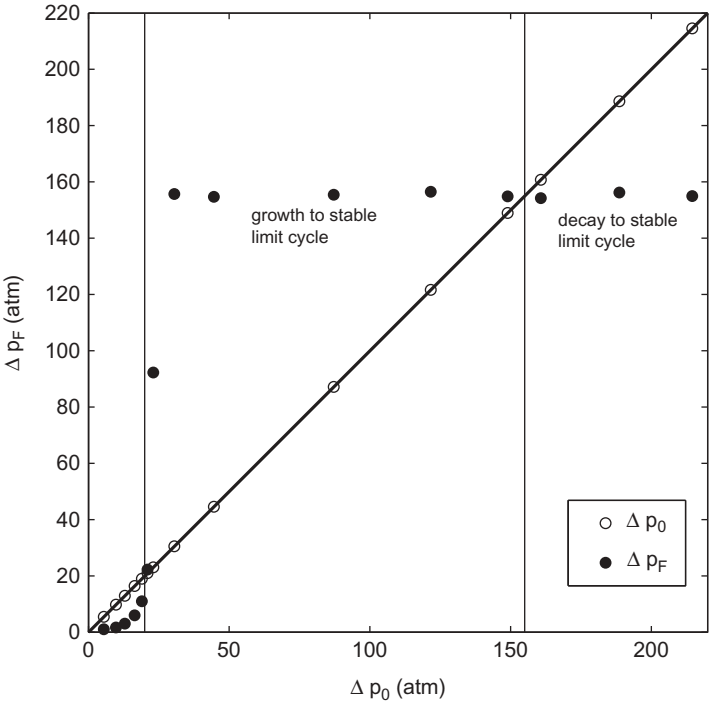


**Figure 9** Oscillation pressure amplitude at 12 cycle times vs. triggering pressure amplitude. [Reprinted from P.P. Popov, A. Sideris, and W.A. Sirignano, "Stochastic modeling of transverse wave instability in a liquid propellant rocket engine," *J. Fluid Mech.*, vol. 745, pp. 62–91, 2014.]

resonant modes that will sum to give an accurate solution. It is unclear which modes and how many modes should be represented. In addition to or instead of the resonant modes, harmonics of primary modes can appear. Also, subharmonics can be generated.

The CFD results of Figure 9 obviously present more information about the dynamic behavior than has been gained from perturbation theory. Perturbation theory can, in principle, handle transient predictions with the emergence of multiscale methods (Kevorkian and Cole, 1996) but those techniques were not used for partial differential equations in the 1960s. They can handle superposition of different resonant modes. However, like classical Galerkin methods and unlike CFD, the weakness is that the modes must be known in advance. Nevertheless, there is some more insight to be gained from perturbation theory. Equations (36), (39), and (40) have been written so that the left side has only linear terms. The nozzle boundary condition in the functional $R\,(p, u_r, u_\theta)$ provides a term with a first time derivative of pressure, which is a damping function for the oscillation. Some of the energy in the oscillation will be lost by nozzle outflow. The term within $R\,(p, u_r, u_\theta)$ having the time derivative of the energy source $E$ can be described as the forcing function for the oscillation. A combustion model based on turbulent jet diffusion flames at the injectors relates $E$ back to pressure, temperature, and velocity. Every term in the functional $S\,(p, u_r, u_\theta)$ is second order or higher in the perturbation series; those terms in $S$ are not dissipative or forcing functions but they can have strong influence on the amplitude, and wave shape for the oscillation. Consequently, there is no major dissipative mechanism other than the nozzle outflow, unlike the cases with shock wave oscillations. Key factors are that every

term on the left side is $O(\epsilon)$ or higher; every term in $R$ is $O(\epsilon M)$ or higher; and every term in $S$ is $O\left(\epsilon^2\right)$ or higher.

Perturbation analysis showed that the nondimensional amplitude $\varepsilon$ of limit-cycle oscillations with shock waves were of the order of the mean-flow Mach number $M$. We can show now that, for continuous wave oscillations, the amplitude parameter $\epsilon = O\left(\sqrt{M}\right)$. This relation was implicit in the results of Sirignano (1964) and Zinn (1968) but were not identified. For simplicity, let us consider a case where the first tangential traveling mode is excited (although the argument and conclusion is not limited to a specific mode). The multiscale perturbation method with coordinate straining will be used. Expand the variables in a perturbation series, e.g., $p = \bar{p} + \epsilon p_1(\phi, \eta, r) + \epsilon^2 p_2(\phi, \eta, r) + \epsilon^3 p_3(\phi, \eta, r) + O\left(\epsilon^4\right)$; $\phi \equiv \omega t - \theta$); $\omega = \omega_0 + \epsilon\omega_1 + \epsilon^2\omega_2 + O\left(\epsilon^3\right)$; and $\eta = \sigma(\varepsilon)\, t$, where $\omega$ and $\eta$ are the frequency and a "slow" time. $\sigma$ goes to zero as $\varepsilon$ goes to zero; in fact, it will be found to go faster.

Consider that, to first order, one obtains $p_1 = [A(\eta)\, cos\phi + B(\eta)\, sin\phi]\, J_1(s_{11} r)$, where $J_1$ is a Bessel function of the first kind and first order while $s_{11}$ is the lowest eigenvalue of that function. The amplitudes $A$ and $B$ are allowed to vary slowly with time to capture the transient behavior while $\phi$ carries the fast time of the oscillation. The use of two time variables produces terms of $O(\epsilon\sigma(\epsilon))$ and higher, which can be added to the right side of the governing partial differential equations; substitution into $R$ gives terms of $O(\varepsilon M)$ and higher; and substitution into $S$ gives terms of $O\left(\varepsilon^2\right)$, $O\left(\varepsilon^3\right)$, and higher. The types of terms appearing on the right side of the wave equation are listed below. Each term would be multiplied by some function of radius $r$, which is not being detailed here. Those multiplying functions can be expanded in a Fourier–Bessel series; the $J_1(s_{11} r)$ term in the series for expansions of the coefficients of $\cos\phi$ and $\sin\phi$ will be of special interest.

$$
\begin{aligned}
&O\left(\varepsilon^2\right): \; A^2 \; ; \; A^2\cos 2\phi \; ; \; AB\sin 2\phi \; ; \; B^2 \; ; \; B^2\cos 2\phi \\
&O(\varepsilon M): \; A\cos\phi \; ; \; A\sin\phi \; ; \; B\cos\phi \; ; \; B\sin\phi \\
&O(\varepsilon\sigma(\varepsilon)): \qquad \frac{dA}{d\eta}\sin\phi \; ; \; \frac{dB}{d\eta}\cos\phi \\
&O\left(\varepsilon^3\right): \; A^3\cos\phi \; ; \; A^3\cos 3\phi \; ; \; A^2B\sin\phi \; ; \; A^2B\sin 3\phi \\
&\qquad\qquad AB^2\cos\phi \; ; \; AB^2\cos 3\phi \; ; \; B^3\sin\phi \; ; \; B^3\sin 3\phi
\end{aligned}
\tag{42}
$$

After substitution and eigenfunction expansion, the terms $J_1(s_{11} r)\cos\phi$ and $J_1(s_{11} r)\sin\phi$ cannot be allowed to remain on the right side of the higher-order wave equations. They are homogeneous solutions to the left side and would prevent a uniformly valid perturbation series from developing. These terms must be collected into two groups and each group must be set to zero. This is accomplished by selecting $\sigma = \varepsilon^2 = M$ so that all $\cos\phi$ and $\sin\phi$ terms on the right side appear at $O\left(\varepsilon^3\right)$. The appearance of nonoscillatory terms means that the average pressure is changed by the nonlinear dynamics. The types of terms appearing here were also found by Zinn (1968) for tangential-mode combustion instability and by Maslen and Moore (1956) in their classical work on nonreacting transverse waves. Maslen and Moore (1956) also examined the effects of wall friction and found that a steady acoustic streaming motion appeared to second order due to the imposed torque.

In setting those two right-side global coefficients to zero, two coupled first-order ordinary differential equations for $A(\eta)$ and $B(\eta)$ result:

$$\frac{dA}{d\eta} = f(A,B) \qquad \frac{dB}{d\eta} = g(A,B) \tag{43}$$

With appropriate initial conditions, these equations describe the growth or decay of the instability with the slow time $\eta$. Of course, both slow time and fast time are converted back to a single time variable. Since the functions $f$ and $g$ are cubic in $A$ and $B$, one or two sets of values of those amplitudes (other than the trivial $A = B = 0$) can produce zero values for the derivatives. These values would mark the unstable limit cycle (i.e., triggering threshold) and the stable limit cycle. Without shock dissipation, the acoustic energy flux at the boundaries must balance globally in the limit-cycle condition; it is expected therefore that $O\left(\varepsilon^2 M\right)$ terms and $O\left(\varepsilon^4\right)$ terms would balance each other.

Major results here are that the nondimensional limit-cycle amplitude $\varepsilon$ is of the order of $\sqrt{M}$ and the nondimensional (using chamber radius and mean sound speed) transient time for development of the high amplitude oscillation will be of the order of $1 / M$. Equivalently, the dimensional transient-time order of magnitude is the chamber radius divided by the mean velocity. Since there are no shock waves for dissipation here, higher amplitude waves result: i.e., $\sqrt{M} > M$ for subsonic mean flow. In fact, the amplitudes for transverse continuous waves are known to be several-fold larger than longitudinal waves, which can form shocks (Harrje and Reardon, 1972). Note that Popov et al. (2014) report a 155 atm peak-to-peak limit-cycle amplitude with a 200 atm mean pressure for a mean flow $M = 0.100$. Then, $\varepsilon = 0.387$ and $\sqrt{M} = 0.316$, which are of the same order of magnitude. Also, a rise above the original 200 atm mean pressure is calculated for the midpoint pressure between the maximum and minimum values in the limit cycle. The transient time for limit-cycle development (an e-folding time) of $1/M$ relates to roughly three cycles of oscillation in that same calculation, which agrees with the finding in the calculation. The Mach number of the mean flow is representative of the strengths of forcing by combustion and damping by nozzle in the chosen examples here. Different parameters can become representative of those critical strengths in other configurations.

### 5.3. General Observations

With regard to the ordering of the terms in an asymptotically correct manner, we have assumed for convenience that the same order applies to both the stable-limit-cycle amplitude and the unstable-limit-cycle amplitude. An interesting possibility worthy of future examination is that different ordering occurs. For example, different powers of $M$ might be appropriate for the two types of limit cycles. This could explain why two distinct solutions were not found in third-order analyses (Sirignano, 1964; Zinn, 1968).

The characteristic times for combustion will affect the likelihood of instability and the amplitude of oscillations. The combustion times have this role because they affect the magnitude of the rate $E$, which comes in phase with pressure. However, the transient time for the oscillation to develop is determined largely by the gasdynamics and is only weakly dependent on the combustion times.

The balance of terms in determining limit-cycle amplitude to lowest order of accuracy has involved linear combustion and nozzle flow terms matched against nonlinear gasdynamic terms for both cases with shocks and without shocks and for both longitudinal and

transverse modes. These linear terms are the lowest-order approximations to the forcing and damping of the oscillation. Nonlinear forcing and damping terms should appear to higher order. Of course, in CFD computations at UCI (Popov et al., 2014; Sirignano and Popov, 2013), the full nonlinear combustion and nozzle effects have been considered. In cases where linear representation serves for a first approximation, the qualitative differences are small between the results using an ad hoc two-parameter combustion model (Crocco and Mitchell, 1969; Mitchell et al., 1969; Sirignano, 1964; Zinn, 1968) and the results using a physics-based description (Popov et al., 2014; Sirignano, 1968; Sirignano and Crocco, 1964; Sirignano and Popov, 2013); essentially two parameters can do reasonably well describing the ratio of the $E$ perturbation to the $p$ perturbation to lowest order.

Culick (2006) describes second-order and third-order perturbation analyses at Caltech (Awad and Culick, 1986; Yang and Culick, 1990; Yang et al., 1990), which never predicted triggering action. This is not inconsistent with the above-described results, which indicated that three types of stability zones could be predicted by any model that predicted the possibility of triggering. That is, by variation of operating parameters, the models of Sirignano (1964), Zinn (1968), Mitchell et al. (1969), and Sirignano and Popov (2013) predicted a neighboring domain of unconditional stability and a neighboring domain of unconditional instability for any bistable domain where triggering occurs. Thus, causes for not predicting triggering could be due to a wrong choice of operational parameters, a poor model, or choice of a combustor configuration not subjected to bistable operation. Culick (2006) suggests that nonlinear gasdynamics by itself is insufficient to develop triggering possibilities, i.e., bistable domains; it is further suggested that nonlinearity in the combustion description is needed to establish the needed limit cycle. Certainly, that suggestion is not consistent with the above-described Princeton asymptotic theory from the 1960s or the recent CFD findings at UCI. For a solid-rocket engine, triggering of combustion instability was predicted by Wicker et al. (1996).

Unstable and stable limit cycles have been predicted to exist together with balance of acoustic energy addition via combustion by the contribution of nonlinear gasdynamic terms. It must be understood that, for cases without shock waves, the nonlinear gasdynamics bring balance, not by direct consequence within the combustor volume, but rather by influence on the acoustic energy efflux through the nozzle. In a test (Sirignano and Popov, 2013) with an artificial example where $E$ is a polynomial in $p$ with no history effect or time lag, the bistable behavior is predicted. A bistable case was found using a relation $E(p)$ where both $E$ and $dE/dp$ were strongly monotonically increasing, positive functions of $p$. This implied that balance with a stable limit cycle could only occur if the gasdynamic terms grew more strongly with increasing pressure than the $E$ combustion term.

Limited experimental results exist for comparison with computations. An interesting program at Purdue University (Shipley et al., 2013) involves a rectangular cross-section combustion chamber with transverse oscillations. For this geometry, shock waves might travel in the transverse direction. In fact, Figure 8 of that paper showing oscillatory pressure profiles indicates the classical result with shocks of steep wavefronts with different steep fronts for travel in each direction. New analyses will have to reflect this different geometry if comparisons are to be made. The experimental design also allows for study of the effect of transverse velocity on the coaxial jet flame from each injector during oscillation. A good computational analysis of this velocity coupling is needed.

The effect of entropy variation in the wave phenomenon described by Eq. (18) is generally neglected. For the inviscid, non-heat-conducting case, this leads to the existence of a velocity potential for the acoustical perturbations, i.e., no vorticity is associated with the

oscillation. However, some damping of the oscillation can be expected from the presence of that entropy term. A rough estimate based on a relation of entropy gain with temperature would yield that the expected magnitude of that entropy term in the wave equation is less than the energy addition rate due to combustion by a multiplicative factor of $(\gamma - 1)/\gamma$. Therefore, unless proven otherwise by a more exact analysis, the neglect of that term should be done with caution.

## 6. CONCLUDING REMARKS

Combustion instability can occur in an engine with spray flow resulting from injection of liquid propellants. The presence of the second phase modifies the wave dynamics but a wave equation can still be constructed describing the nonlinear acoustics. The wave equation contains terms reflecting the exchanges of mass, moment, and energy between the phases; however, the highest derivatives in the equation are identical to those for the single-phase wave equation.

The combustion instability phenomena present a multi-scale problem. Various length and time scales result from acoustics; kinematic waves; and the processes for injection, vaporization, mixing, and oxidation. The Sensitive-Time-Lag Theory and other heuristic approaches allow the bypass of treatment of the smaller scales associated with combustion. Mathematical and computational approaches that address all of the physically important scales are desired for the future and are beginning to appear.

Combustion instability becomes more likely when a change in operational parameters causes the fractional perturbation in the energy release rate $\Delta E/\bar{E}$ to increase for a given fractional change in pressure $\Delta p/\bar{p}$. The chemical-kinetic-controlled combustion shows this non-intuitive effect for the gas rocket engine where near-stoichiometric operation can be more stable than off-stoichiometric operation. This behavior has implications for lean-combustion systems.

Ubiquitous examples exist where the most unstable domain has a controlling characteristic time that aligns well with the resonant frequency; see the results of Figures 3 and 4. Cases of poor alignment can explain stable operation. See Figure 6 and the explanation for stable operation of $H_2 - O_2$ systems.

Bistable operational domains are shown to be present in some systems, making nonlinear triggering of an instability a possibility. In these domains, both a stable limit cycle and an unstable limit cycle (triggering threshold) exist. The bistable region typically lies between an unconditionally stable zone and an unconditionally unstable zone in operational parameter space.

For oscillations with shock waves, the associated dissipation keeps the nondimensional limit-cycle amplitude to the order of the mean-flow Mach number $M$. A perturbation analysis up to second order in amplitude is sufficient here for the lowest approximation to amplitude. Comparison with an experiment verified this asymptotic ordering. For continuous waves, larger amplitudes of the order of $\sqrt{M}$ appear with a nondimensional transient development time of the order of $1/M$. A third-order analysis is required to estimate the amplitude. In a limited comparison with CFD results, support for this ordering was found. For the cases discussed, the Mach number of the mean flow was representative of the strengths of forcing by combustion and damping by nozzle. In other cases, different parameters can become representative of those critical strengths.

For longitudinal and transverse modes of oscillation with and without shock waves, the primary balance in determining limit cycles comes between linear terms representing

forcing by combustion and damping by nozzle and nonlinear gasdynamic terms. For higher-order refinement of the description, nonlinear forcing and damping terms can become relevant.

Some important problems remain related to driving mechanisms for combustion instability; a few examples can be briefly presented. (i) The interactions of the acoustic oscillation with the turbulent structures needs to be understood better. When is the coupling well represented as one-way? That is, when does the acoustic field influence the turbulence without the turbulence significantly affecting the acoustics? We allow here for indirect influence through the combustion process; i.e., acoustics affect turbulence, which then influences the combustion driving mechanism. (ii) More studies are needed about the driving mechanisms for continuous operation at very high pressures and also for intermittent high pressure operation during peak portions of the acoustic oscillation period. It must be determined when two phases can exist, which cannot be determined a priori by comparing the critical pressure and temperature for each propellant to the operating conditions. Studies of instantaneous and local mixture critical values are needed. (iii) The response of the combustion processes to transverse waves can be very important but is not well understood. In summary, challenging opportunities for research related to combustion instability driving mechanisms remain to be addressed further.

## FUNDING

This research was supported by the Air Force Office of Scientific Research under Grant FA9550-12-1-0156, with Dr. Mitat Birkan as the Program Manager.

## NOMENCLATURE

| | |
|---|---|
| $A$ | pre-exponential factor |
| $A_t$, $A_c$ | cross-sectional area of nozzle throat and capture flow |
| $A$, $B$, $C$, $D$ | constants in the generic nonlinear differential for $f\ (\theta)$ |
| $a$ | speed of sound |
| $a_s$ | acceleration of liquid stream |
| $a$,$b$ | constants in cubic equation of state |
| $Bo$ | Bond number |
| $c_p$ | specific heat under constant pressure |
| $c_v$ | specific heat under constant volume |
| $D$ | mass diffusivity |
| $E$ | energy conversion rate per unit volume |
| $E_A$ | activation energy |
| $e$ | specific internal energy |
| $F$ | functional in wave function equation |
| $F_{Di}$ | aerodynamic force on droplets per unit mixture volume |
| $f$ | wave function |
| $G$ | response factor |
| $H$ | collection of terms in Eq. (29) |
| $h$ | specific enthalpy |
| $n$ | droplet number density |
| **n** | interaction index of Sensitive-Time-Lag Theory |
| $p$ | pressure |
| $Q$ | heat of combustion |

| | |
|---|---|
| $R$ | specific gas constant |
| $R$ | combustion chamber radius |
| $R$ | source term in wave equation |
| $R_u$ | universal gas constant |
| $r$, $r_i$ | global rate, rate of process $i$ |
| $S$ | source term in equation |
| $s$ | specific entropy |
| $\mathbf{T}$ | cycle period |
| $T$ | temperature |
| $t$ | time |
| $u$, $v$, $u_i$ | velocity |
| $U_s$ | characteristic velocity of liquid stream |
| $v$ | specific volume |
| $We$ | Weber number |
| $x_i$ | Cartesian coordinates |
| $Y_m$ | mass fraction of species $m$ |
| $\rho$ | density |
| $\rho_l$ | liquid density |
| $\bar{\rho}$ | mass of gas per unit volume in two-phase flow |
| $\sigma$ | asymptotic order for slow time |
| $\sigma_s$ | surface tension for liquid stream |
| $\tau$ | time lag |
| $\tau_M$, $\tau_R$ | characteristic times for mixing and chemical reaction |
| $\tau_{ij}$ | viscous stress tensor |
| $\Phi$ | viscous dissipation |
| $\omega_m$ | reaction rate for species $m$ |

## Superscripts

| | |
|---|---|
| $'$ | perturbation quantity |
| $\bar{}$ | steady-state value |
| $\tau$ | time-lag applied to argument of term |

## Subscripts

| | |
|---|---|
| $c$ | critical thermodynamic quantity |
| $i$, $j$, $x$, $y$, $r$, $\theta$ | indices for vector direction |
| $m$ | index for chemical species |
| 1, 2, 3, . . . | order of perturbation quantity |

## REFERENCES

Abramzon, B., and Sirignano, W.A. 1989. Droplet vaporization model for spray combustion calculations. *Int. J. Heat Mass Transfer*, **32**(9), 1605–1618.

Awad, E., and Culick, F. 1986. On the existence and stability of limit cycles for longitudinal acoustic modes in a combustion chamber. *Combust. Sci. Technol.*, **46**, 195–222.

Bhatia, R., and Sirignano, W.A. 1991. A one-dimensional analysis of liquid-fueled combustion instability. *J. Propul. Power*, **7**, 953–961.

Bowman, C. 1967. Experimental investigation of high-frequency longitudinal combustion instability in gaseous propellant rocket motors. Report 66–2725. Air Force Office of Scientific Research.

Bowman, C., Glassman, I., and Crocco, L. 1965. Combustion instability in gas rockets. *AIAA J.*, **3**, 1981.

Continillo, G., and Sirignano, W.A. 1988. Numerical study of multicomponent fuel spray flame propagation in a spherical closed volume. *Symp. (Int.) Combust.*, **22**, 1941–1949.

Crocco, L. 1972. Coordinate perturbation and multiple scale in gasdynamics. *Philos. Trans. R. Soc.*, **272**, 275–301.

Crocco, L., and Cheng, S.-I. 1953. High frequency combustion instability in rockets with distributed combustion. *Symp. (Int.) Combust.*, **4**, 865–880.

Crocco, L., and Cheng, S.-I. 1956. *Theory of Combustion Instability in Liquid Propellant Rocket Motors*, AGARD Monograph 8, Buttersworth, London.

Crocco, L., and Mitchell, C.E. 1969. Nonlinear periodic oscillations in rocket motors with distributed combustion. *Combust. Sci. Technol.*, **1**, 147–169.

Crocco, L., and Sirignano, W.A. 1966. Effects of transverse velocity components on the nonlinear behavior of short nozzles. *AIAA J.*, **4**, 1428–1430.

Crocco, L., and Sirignano, W.A. 1967. *Behavior of Supercritical Nozzle Under Three Dimensional Oscillatory Conditions*. AGARDograph No. 117, North Atlantic Treaty Organization, Neuilly-Sur-Seine, France.

Culick, F. 1976. Nonlinear behavior of acoustic waves in combustion chambers. *Acta Astronaut.*, **3**, 715–734.

Culick, F.E.C. 1967. Calculation of the admittance function for a burning surface. *Proceedings of the Third ICRPG Combustion Conference*, CPIA Publication No. 138, Vol. **1**, p. 307.

Culick, F.E.C. 2006. *Unsteady Motions in Combustion Chambers for Propulsion Systems*. AGARDograph AG-AVT-039, North Atlantic Treaty Organization, Neuilly-Sur-Seine, France.

Delplanque, J.-P., and Sirignano, W.A. 1993. Numerical study of transient vaporization of an oxygen droplet at sub- and super-critical conditions. *Int. J. Heat Mass Transfer*, **36**, 303–314.

Delplanque, J.-P., and Sirignano, W.A. 1994. Boundary layer stripping effects on droplet transcritical convective vaporization. *Atomization Sprays*, **4**, 325–349.

Delplanque, J.-P., and Sirignano, W.A. 1995. Transcritical vaporization and combustion of lox droplet arrays in a convective environment. *Combust. Sci. Technol.*, **105**, 327–344.

Delplanque, J.-P., and Sirignano, W.A. 1996. Transcritical liquid oxygen droplet vaporization: Effect on rocket combustion instability. *J. Propul. Power*, **12**, 349–357.

Denison, R., and Baum, E. 1961. A simplified model for unstable burning in solid propellants. *ARS J.*, **31**, 112.

Godsave, G.A.E. 1953. Studies of the combustion of drops in a fuel spray: The burning of single drops of fuel. *Symp. (Int.) Combust.*, **4**, 818–830.

Harper, E.Y., Grube, G.W., and Chang, I.-D. 1972. On the breakup of accelerating liquid drops. *J. Fluid Mech.*, **52**, 565–591.

Harrje, D., and Reardon, F. 1972. Liquid propellant rocket combustion instability. NASA SP194. U.S. Government Printing Office.

Heidmann, M.F., and Wieber, P. 1965. Analysis of *n*-heptane vaporization in unstable combustor with travelling transverse oscillations. NASA Technical Note 3424.

Hsiao, G.C., Meng, H., and Yang, V. 2011. Pressure-coupled vaporization response of n-pentane fuel droplet at subcritical and supercritical conditions. *Proc. Combust. Inst.*, **33**, 1997–2003.

Hsieh, K., Shuen, J., and Yang, V. 1991. Droplet vaporization in high pressure environments: I. near-critical conditions. *Combust. Sci. Technol.*, **76**(1–3), 111–132.

Jackson, T.L. 2012. Modeling of heterogeneous propellant combustion: A survey. *AIAA J.*, **50**(5), 993–1006.

Kevorkian, J.K., and Cole, J.D. 1996. *Multiple Scale and Singular Perturbation Methods*, Springer-Verlag, New York.

Krier, H., T'ien, J., Sirignano, W.A., and Summerfield, M. 1968. Non-steady burning phenomenon in solid propellants: Theory and experiments. *AIAA J.*, **6**, 278.

Liepmann, H., and Roshko, A. 1957. *Elements of Gasdynamics*, John Wiley and Sons, New York.

Maslen, S.H., and Moore, F.K. 1956. On strong transverse waves without shocks in a circular cylinder. *J. Aeronaut. Sci.*, **23**(6), 583–593.

Minorsky, N. 1962. *Nonlinear Oscillations*, Van Nostrand, Princeton, NJ.

Mitchell, C.E., Crocco, L., and Sirignano, W.A. 1969. Nonlinear longitudinal instability in rocket motors with concentrated combust. *Combust. Sci. Technol.*, **1**, 35–63.

Popov, P.P., Sideris, A., and Sirignano, W.A. 2014. Stochastic modeling of transverse wave instability in a liquid propellant rocket engine. *J. Fluid Mech.*, **745**, 62–91.

Priem, R.J., and Heidmann, M.F. 1960. Propellant vaporization as a design criterion for rocket-engine combustion chambers. NASA Technical Report R-67.

Ranger, A.A., and Nicholls, J.A. 1972. Atomization of liquid droplets in a convective gas stream. *Int. J. Heat Mass Transfer*, **15**, 1203–1211.

Reardon, F.H., Crocco, L., and Harrje, D.T. 1964. Velocity effects in transverse mode liquid propellant rocket combustion instability. *AIAA J.*, **12**, 1631–1641.

Roh, T.-S., Tseng, I.-S., and Yang, V. 1995. Effects of acoustic oscillations on flame dynamics of heterogeneous propellants in rocket motors. *J. Propul. Power*, **11**(4), 640–650.

Schmitt, T., Mery, Y., Boileau, M., and Candel, S. 2011. Large-eddy simulation of oxygen/methane flames under transcritical conditions. *Proc. Combust. Inst.*, **33**, 1383–1390.

Shipley, K., Morgan, C., Anderson, W.E., Harvazinski, M.E., and Sankaran, V. 2013. Computational and experimental investigation of transverse combustion instabilities. Presented at the 49th AIAA/ASME/SAE/ASEE Joint Propulsion Conference and Exhibit, San Jose, CA, July 15–17.

Sirignano, W.A. 1964. Theoretical study of nonlinear combustion instability: Longitudinal mode. PhD dissertation. Princeton University Department of Aerospace and Mechanical Sciences Report No. 677, Princeton, NJ.

Sirignano, W.A. 1968. A theory of axial-mode shock-wave oscillations in a solid-rocket combustor. *Symp. (Int.) Combust.*, **12**, 129–137.

Sirignano, W.A. 1972. Non linearita dei risonatori di Helmholtz. *L'Aerotecnica Missili e Spazio*, **51**(4), 1256–1265.

Sirignano, W.A. 2005a. Corrigendum to 'Volume averaging for the analysis of turbulent spray flows' [*Int. J. Multiphase Flow*, **31**, 675–705]. *Int. J. Multiphase Flow*, **31**, 867.

Sirignano, W.A. 2005b. Volume averaging for the analysis of turbulent spray flows. *Int. J. Multiphase Flow*, **31**, 675–705.

Sirignano, W.A. 2010. *Fluid Dynamics and Transport of Droplets and Sprays*, 2nd ed., Cambridge University Press, New York.

Sirignano, W.A. 2014. Advances in droplet array combustion theory and modelling. *Prog. Energy Combust. Sci.*, **42**, 54–86.

Sirignano, W.A., and Crocco, L. 1964. A shock wave model of unstable rocket combustors. *AIAA J.*, **2**, 1285–1296.

Sirignano, W.A., and Delplanque, J.P. 1999. Transcritical vaporization of liquid fuels and propellants. *J. Propul. Power*, **15**(6), 896–902.

Sirignano, W.A., and Popov, P. 2013. Two-dimensional model for liquid-rocket transverse combustion instability. *AIAA J.*, **51**(12), 2919–2934.

Spalding, D.B. 1953. The combustion of liquid fuels. *Symp. (Int.) Combust.*, **4**, 847–864.

Strahle, W.C. 1965a. Periodic solutions to a convective droplet burning problem: The stagnation point. *Symp. (Int.) Combust.*, **10**, 1315–1325.

Strahle, W.C. 1965b. Unsteady laminar jet flame at large frequencies of oscillation. *AIAA J.*, **3**, 957.

Strahle, W.C. 1965c. Unsteady reacting boundary layer on a vaporizing flat plate. *AIAA J.*, **3**, 1195.

Strahle, W.C. 1967. High frequency behavior of laminar jet flame subjected to transverse sound waves. *Symp. (Int.) Combust.*, **11**, 747–754.

Tang, P.K., Harrje, D.T., and Sirignano, W.A. 1973. Experimental verification of the energy dissipation mechanism in acoustic dampers. *J. Sound Vib.*, **26**(2), 263–267.

Tang, P.K., and Sirignano, W.A. 1973. Theory of a generalized helmholtz resonator. *J. Sound Vib.*, **26**(2), 247–262.

T'ien, J., and Sirignano, W.A. 1971. Unsteady thermal response of the condensed phase fuel to a reacting gaseous boundary layer. *Symp. (Int.) Combust.*, **13**, 529–539.

Tong, A., and Sirignano, W.A. 1989. Oscillatory vaporization of fuel droplets in unstable combustor. *J. Propul. Power*, **5**(3), 257–261.

Tsien, H.S. 1952. The transfer function of rocket nozzles. *ARS J.*, **22**, 139–143.

Westbrook, C.K., and Dryer, F.L. 1984. Chemical kinetic modeling of hydrocarbon combustion. *Prog. Energy Combust. Sci.*, **10**, 1–57.

Wicker, J.M., Greene, W.D., Kim, S.I., and Yang, V. 1996. Triggering of longitudinal combustion instabilities in rocket motors. *J. Propul. Power*, **12**(6), 1148–1158.

Williams, F.A. 1958. Spray combustion and atomization. *Phys. Fluids*, **1**(6), 541–545.

Williams, F.A. 1959. Spray combustion theory. *Combust. Flame*, **3**(2), 215–228.

Williams, F.A. 1960. On the assumptions underlying droplet vaporization and combustion theories. *J. Chem. Phys.*, **33**(1), 133–144.

Williams, F.A. 1965. Response of a burning fuel plate to sound vibrations. *AIAA J.*, **3**(11), 2112–2124.

Williams, F.A. 1985. *Combustion Theory*, 2nd ed., The Benjamin/Cummings Publishing Company, Inc., Reading, MA.

Yang, V. 2000. Modeling of supercritical vaporization, mixing, and combustion processes in liquid-fueled propulsion systems. *Proc. Combust. Inst.*, **33**, 925–942.

Yang, V., and Anderson, W.E. 1995. *Liquid Rocket Engine Combustion Instability* (Progress in Astronautics and Aeronautics 169), AIAA, Reston, VA.

Yang, V., and Culick, F. 1990. On the existence and stability of limit cycles for transverse acoustic oscillations in a cylindrical combustion chamber. 1: Standing modes. *Combust. Sci. Technol.*, **72**, 37–65.

Yang, V., Kim, S., and Culick, F. 1990. Triggering of longitudinal pressure oscillations combustion chambers. I: Nonlinear gasdynamics. *Combust. Sci. Technol.*, **75**, 183–214.

Yang, V., and Lin, N.N. 1994. Vaporization of liquid oxygen (LOX) droplets at supercritical conditions. *Combust. Sci. Technol.*, **97**, 247–270.

Zinn, B.T. 1968. A theoretical study of nonlinear combustion instability in liquid-propellant rocket engines. *AIAA J.*, **6**, 1966–1972.

Zinn, B.T., and Crocco, L. 1968. Nozzle boundary condition in nonlinear rocket instability problem. *Acta Astronaut.*, **13**, 489–496.

Zinn, B.T., and Powell, E.A. 1971. Nonlinear combustion instability in liquid-propellant rocket engines. *Symp. (Int.) Combust.*, **13**, 491–503.

Zong, N., and Yang, V. 2006. Cryogenic fluid jets and mixing layers in transcritical and supercritical environments. *Combust. Sci. Technol.*, **178**(1–3), 193–227.